NASA Contractor Report 181649

ICASE REPORT NO. 88-20

ICASE

NUMERICAL EXPERIMENTS ON THE STABILITY OF CONTROLLED BOUNDARY LAYERS

Thomas A. Zang

M. Y. Hussaini

Contract No. NAS1-18107
March 1988

INSTITUTE FOR COMPUTER APPLICATIONS IN SCIENCE AND ENGINEERING
NASA Langley Research Center, Hampton, Virginia 23665

Operated by the Universities Space Research Association

National Aeronautics and
Space Administration

Langley Research Center
Hampton, Virginia 23665

NUMERICAL EXPERIMENTS ON THE STABILITY OF CONTROLLED BOUNDARY LAYERS

Thomas A. Zang*
NASA Langley Research Center
Hampton, Virginia

M. Y. Hussaini**
Institute for Computer Applications in Science and Engineering
NASA Langley Research Center
Hampton, Virginia

Abstract

Nonlinear simulations are presented for instability and transition in parallel water boundary layers subjected to pressure gradient, suction, or heating control. In the nonlinear regime, finite amplitude two-dimensional Tollmien-Schlichting waves grow faster than is predicted by linear theory. Moreover, this discrepancy is greatest in the case of heating control. Likewise, heating control is found to be the least effective in delaying secondary instabilities of both the fundamental and subharmonic type. Flow-field details (including temperature profiles) are presented for both the uncontrolled boundary layer and the heated boundary layer.

This research was supported by the National Aeronautics and Space Administration under NASA Contract No. NAS1-18107 while the second author was in residence at the Institute for Computer Applications in Science and Engineering (ICASE), NASA Langley Research Center, Hampton, VA 23665.

* Research Scientist, Computational Methods Branch, High-Speed Aerodynamics Division.
**Chief Scientist.

Introduction

Laminar flow control (LFC) techniques have been investigated extensively both experimentally and theoretically. Most of the theoretical work has relied on linear theory and asymptotic methods. Since the literature on LFC is so vast, we simply refer the reader to the survey article by Hefner and Bushnell (1979) and cite specifically only that work which is especially pertinent to our own. Wazzan, Okamura, and Smith (1968) have performed an extensive study of the linear stability of the heated, parallel, water boundary layer. They ignored the temperature fluctuations and found that wall heating increased the critical Reynolds number. Lowell and Reshotko (1974) included the effects of temperature perturbations in the linear stability analysis and concluded that they did not significantly change the results. Strazisar, Reshotko, and Prahl (1977) and Barker (1979) verified experimentally the linear stability results for low amplitude two-dimensional Tollmien-Schlichting-Schubauer (TS) waves. They found that the parallel theory gave an adequate description of the neutral curve except near the critical Reynolds numbers for slightly heated flows.

However, even if high intensity bypass mechanisms (Morkovin (1969)) are not involved, linear theory describes only the first stage of transition--the slow growth of the primary, TS instability. Subsequent stages are due to nonlinear interactions. A wide variety of asymptotic methods have been used to describe secondary instabilities arising from the interaction of three-dimensional disturbances with the primary 2-D TS wave. Of these methods Floquet theory (see the review by Herbert (1988)) has been particularly successful in clarifying the secondary instabilities of both fundamental and subharmonic type in channels and boundary layers. These methods have yet to be applied to controlled boundary layers.

Experimental (Klebanoff, Tidstrom, and Sargent (1962), Kovasznay, Komoda, and Vasudeva (1962), Hama and Nutant (1963), Wortmann (1977), and Williams, Fasel, and Hama (1984)) and numerical (Wray, Hussaini, and Degani (1977), Wray and Hussaini (1980, 1984), Orszag and Patera (1983), Kleiser and Schumann (1984)) work have demonstrated that the fundamental secondary instability for uncontrolled boundary layers leads to the emergence of periodic lambda vortices and to the development of detached shear layers which ride on top of them. The lambda vortices originate near the critical layers where the wave speed of the 2-D mode matches the local mean flow speed. They originate because of the secondary instability and they intensify because of nonlinear self-induction effects. The detached shear layer arises because the mean flow must traverse the vortices. Subsequent developments are at best only qualitatively understood: the shear layers roll up and shed discrete vortices (Hama and Nutant (1963)) and eventually turbulence ensues. The lambda vortices and the detached shear layers are strongly three-dimensional, time-dependent structures. Numerical simulations have the potential to provide a theoretical prediction of the tertiary instabilities of these structures without resorting to drastic simplifications, such as assumptions of two-dimensionality, weak three-dimensionality, or quasi-steadiness. Such predictions via numerical simulations, however, are quite costly and have been furnished only for channel flow (Gilbert and Kleiser (1986), Krist and Zang (1987)).

Experiments on the subharmonic secondary instability have not yet produced such great detail on the evolution of the lambda vortices. Likewise, most numerical simulations of subharmonic transition (Spalart and Yang (1987)) have proceeded only to the stage at which these structures emerge. Moreover, little or no experimental work has been done on either secondary instability in controlled boundary layers.

In this paper we apply direct numerical simulations of the time-dependent, incompressible Navier-Stokes equations to explore a variety of non-linear effects in boundary layers subjected to pressure gradient, suction, or heating controls. The LFC technique are here limited to passive, spatially and temporally uniform controls, with the emphasis on heating control for water boundary layers. The effect of finite amplitudes on the growth of 2-D TS waves is examined first. Then a comparison is made of the effect of the LFC techniques on both the fundamental and subharmonic secondary instabilities. Next, flow visualizations are presented for the early stages of the tertiary instability. Finally, the crucial role played by longitudinal vortices in the fundamental instability is illustrated.

Formulation

The boundary layer on a flat plate is illustrated in Figure 1. The streamwise, normal, and spanwise directions are denoted by x, y, and z, respectively. The displacement thickness δ^* increases in the streamwise direction. At any distance x_0 from the leading edge, one can define a Reynolds number Re based on the velocity u_∞ and kinematic viscosity ν_∞ in the free stream and the local displacement thickness.

The transition process of the growing boundary layer is influenced by significant non-linear, three-dimensional and non-parallel effects. Unfortunately, existing computer resources are only adequate for treating two out of these three effects. A common compromise is to study the parallel boundary layer (see Figure 2) instead of the true, growing one. Here the focus is on the vicinity of some point x_0 (see Figure 1) and the approximation is that

the displacement thickness remains constant (in x) at the value $\delta^*_{x_0}$; the mean flow is strictly in the streamwise direction and is given by $\underline{u}_0(x,y,z,t) = (u_0(y),0,0)$, where $u_0(y)$ is the mean velocity profile which follows from the similar boundary-layer equations at x_0. As a consequence, only the non-linear and the three-dimensional effects are taken into account. The neglect of the non-parallel effects should be serious only if there is appreciable growth on the scale (λ_{TS}) of the Tollmien-Schlichting (TS) waves. Since the mean flow in the parallel boundary layer is uniform in x, a Fourier approximation in x is highly accurate; moreover, only one spatial wavelength need be resolved for the temporal transition problem. Thus, highly resolved computations can be performed, well into the strongly non-linear regime.

Figure 3 depicts three types of laminar flow control (LFC) techniques. The dimensionless parameters describing self-similar solution of the Falkner-Skan boundary layer equations are defined in the figure. These are β for pressure gradient, F_w for suction, and τ for heating. In the last case, the free stream and wall temperatures, denoted by T_∞ and T_w, respectively, (and given in degrees Kelvin), differ and the kinematic viscosity depends upon the temperature T.

Lengths are scaled by the displacement thickness at x_0, velocities by the free-stream velocity at x_0, and the density is taken to be constant at 1 gm/cm^3. The Navier-Stokes equations for the dimensionless variables are used in the rotation form

$$\underline{u}_t + \underline{\omega} \times \underline{u} = -\nabla P + \frac{1}{Re} \nabla \cdot [\mu(\nabla \underline{u} + \nabla \underline{u}^T)] + \underline{F}_{\underline{u}} \qquad (1)$$

$$\theta_t + \underline{u} \cdot \nabla\theta = \frac{1}{Pr}\frac{1}{Re}\nabla \cdot (\kappa\nabla\theta) + F_\theta \tag{2}$$

$$\nabla \cdot \underline{u} = 0 \tag{3}$$

where $\theta = (\bar{T} - \bar{T}_\infty)/(\bar{T}_w - \bar{T}_\infty)$, $Re = \bar{u}_\infty\bar{\delta}^*/\bar{\nu}_\infty$, $Pr = \bar{\mu}_\infty\bar{C}_{p\infty}/\bar{\kappa}_\infty$, $\mu = \bar{\mu}/\bar{\mu}_\infty$, $\kappa = \bar{\kappa}/\bar{\kappa}_\infty$,

$$\begin{aligned} \underline{F}_{\underline{u}} &= -\frac{1}{Re}\frac{\partial}{\partial y}\left(\mu_0 \frac{\partial u_0}{\partial y}\right)\hat{i} \\ F_\theta &= -\frac{1}{Pr}\frac{1}{Re}\frac{\partial}{\partial y}\left(\kappa_0 \frac{\partial \theta_0}{\partial y}\right) \end{aligned} \tag{4}$$

and $\bar{C}_p(\bar{T})$ is held fixed at its value at $\bar{T}_\infty$. The forcing functions $\underline{F}_{\underline{u}}$ and F_θ are applied for consistency with the parallel flow assumption.

The boundary conditions are

$$\begin{aligned} &\underline{u} = 0 && \text{at } y = 0 \\ &\theta = 1 \\ &\underline{u} = (1,0,0) && \text{at } y = \infty \\ &\theta = 0 \end{aligned} \tag{5}$$

along with periodicity in x with period L_x and periodicity in z with period L_z. The empirical formulas employed are those recommended by Lowell and Reshotko (1974):

$$\bar{\mu}(\bar{T}) = 1.002\ 10^{-r(\bar{T})} \times 10^{-2}\ \text{gm/cm-sec}$$

$$r(\bar{T}) = \left| 1.370 + 8.36 \times 10^{-4}(\bar{T}-293) \right| (\bar{T}-293)/(\bar{T}-164)$$

$$\bar{\kappa}(\bar{T}) = [-9.901 + 0.1002\ \bar{T} - 1.874 \times 10^{-4}\ \bar{T}^{2} + 1.040 \times 10^{-7}\ \bar{T}^{3}] \times 10^{-3}$$

joule/sec-cm-^{0}K

$$\bar{C}_{p}(\bar{T}) = [2.140 - 9.68 \times 10^{-3}\ \bar{T} + 2.69 \times 10^{-5}\ \bar{T}^{2} - 2.42 \times 10^{-8}\ \bar{T}^{3}]$$

$$\times\ 4.184\ \text{joule/gm} - {}^{0}\text{K}, \qquad (6)$$

where $\bar{T}$ is in ^{0}K. The Prandtl number characteristic of water is Pr = 7.

All of the results in this paper are for $\bar{T}_{\infty} = 293^{0}$K and for $1 \leq \tau \leq 1.1$. Over this range $\bar{C}_{p}(\bar{T})$ varies by less than 0.1% and the density is within 1% of being constant. On the other hand, $\bar{\mu}(\bar{T})$ changes by as much as 50% and $\bar{\kappa}(\bar{T})$ by nearly 7%. Note that viscous dissipation has been neglected in the temperature equation. This is a small correction in the heated cases considered below, which have Eckert numbers $[\bar{u}_{\infty}^{2}/(\bar{C}_{p_{\infty}}(\bar{T}_{w}-\bar{T}_{\infty}))]$ smaller than 10^{-2}. The term $\nabla\cdot(\mu\nabla\underline{u}^{T})$ vanishes if μ is constant (in $\underline{x}$) and has only a minor effect (below the 1% level) on the heated cases, as determined by comparing simulations made both with and without this term.

One of the Reynolds numbers chosen for the present investigation of nonlinear stability was 8950. (Some linear theory results were reported for this Reynolds number by Lowell and Reshotko (1974).) The free stream temperature was 293^{o}K. The amounts of pressure gradient, suction, and heating were chosen so that the flow was neutrally stable. (The linear theory results for the heated case did not include the temperature fluctuations.) The mean flows of both the controlled and uncontrolled cases are displayed in Figure 5, and

the parameters of the least stable 2-D modes are included in Table 1. The characteristics of the least stable linear modes of the heated case differ appreciably from those of the pressure gradient and suction controls. As was observed by Wazzan, et al., there are destabilizing effects in the heated case due to the vertical gradients of μ and κ.

The use of the LFC techniques has a dramatic effect upon the actual displacement thickness of the boundary layer. This is quantified in Table 2. The Reynolds number based on the displacement thickness of the corresponding uncontrolled boundary layer is also listed there. Note that in terms of the growing boundary layer, the controlled cases correspond to different positions x_0, with the pressure gradient case having the greatest distance from the leading edge and the uncontrolled case the least.

Most nonlinear transition calculations have used initial conditions consisting of the mean flow, plus a two-dimensional TS wave and two three-dimensional (oblique) waves:

$$\begin{aligned} \underline{u}(\underline{x},0) = \mathrm{Re}\{&\underline{u}_0(y) + \varepsilon_{2D}\underline{u}_{2D}(y)e^{i\alpha_x x} \\ &+ \tfrac{1}{2}\varepsilon_{3D}\underline{u}^{+}_{3D}(y)e^{i[(\alpha_x/s_x)x+\alpha_z z]} \\ &+ \tfrac{1}{2}\varepsilon_{3D}\underline{u}^{-}_{3D}(y)e^{i[(\alpha_x/s_x)x-\alpha_z z]}\} \end{aligned} \tag{7}$$

where $\underline{u}_{2D(y)}$ and $\underline{u}^{\pm}_{3D}(y)$ are the least stable linear modes for the given real wavenumbers α_x and α_z, and the integer s_x is 1 or 2. These eigenfunctions are normalized so that their maximum streamwise amplitudes are 1. The 3-D waves are either themselves TS waves (solutions to the Orr-

Sommerfeld equation) or else Squire modes (eigenmodes of the vertical vorticity equation (Herbert (1983)). This particular combination of 3-D modes, with waves α_z and $-\alpha_z$, generates streamwise vorticity patterns that resemble those of the Benney-Lin (1960) mechanism.

Numerical Methods

In this work, numerical methods are needed for three problems. The mean flow is calculated from the Falkner-Skan boundary layer equations via a fourth-order finite-difference scheme (Malik, Chuang, and Hussaini (1982)). The linear eigenmodes (and linear stability properties) are computed by a Chebyshev tau method (Orszag (1971)). The mean flow and the linear eigenfunctions are used for the initial conditions of the direct simulation.

The time dependent Navier-Stokes equations are solved by a Fourier-Chebyshev collocation method, using Fourier series in x and z and Chebyshev polynomials (with an algebraic stretching) in y. The velocity has the Fourier series representation

$$\underline{u}(\underline{x},t) = \sum_{\hat{k}_x=-N_x/2}^{N_x/2-1} \sum_{\hat{k}_x=-N_x/2}^{N_x/2-1} \hat{\underline{u}}_{k_x,k_z}(y,t) e^{[(\hat{k}_x/s_x)\alpha_x x + (\hat{k}_z/s_z)\alpha_z z]} \tag{8}$$

where α_x and α_z are the fundamental wavenumbers in the streamwise and spanwise directions respectively. The fundamental wavelengths in these directions are given by $L_x = 2\pi/\alpha_x$ and $L_z = 2\pi/\alpha_z$, respectively. The imposed periodicity lengths are $s_x L_x$ and $s_z L_z$, where s_x and s_z are

integers which specify the number of subharmonics that are permitted in each direction. (In most cases presented in this paper $s_x = s_z = 1$.) The rational numbers $k_x = \hat{k}_x/s_x$ and $k_z = \hat{k}_z/s_z$ label the Fourier wavenumbers in the numerical representations with respect to the fundamental wavenumbers α and β. The velocity also has the Chebyshev series representation

$$\underline{u}(\underline{x},t) = \sum_{n=0}^{N_y} \tilde{\underline{u}}_n(x,z,t)T_n(\xi) \tag{9}$$

where a mapping $y = y(\xi)$ is employed from $[-1,1]$ to $(0,\infty)$. Of course, a fully Fourier-Chebyshev representation is also available. The notation is straightforward: a triple sum over k_x, n, k_z with respect to the coefficients $\tilde{u}_{k_x,n,k_z}$ times the Fourier-Chebyshev basis functions.

The algorithm used for the boundary-layer simulations is based upon the improved splitting method devised by Zang and Hussaini (1986) for channel flow simulations. The first (velocity) step accounts for the advection and diffusion terms. Although the simulations presented in this paper used the rotation form of the incompressible Navier-Stokes equations, recent work indicates that the skew-symmetric form is more accurate (see Zang (1988)). The advection and horizontal diffusion terms are advanced in time via a low-storage third-order Runge-Kutta method while the normal viscous term is advanced with a Crank-Nicolson method. (The temperature equation is also integrated in this step.) The second (pressure) step enforces the incompressibility constraint. The boundary conditions in the velocity step are chosen to minimize the slip velocity which is present after the pressure step. More details are given by Zang and Hussaini (1986). Chapter 7 of the book by Canuto, Hussaini, Quarteroni, and Zang (1988) contains an exhaustive discussion of spectral methods for simulations of incompressible flow.

Several aspects of the boundary-layer implementation of this algorithm are worth noting. Asymptotic boundary conditions (Malik, Zang, and Hussaini (1985)) were enforced at $y = y_{max}$ by requiring that

$$\frac{d}{dy}\hat{u}_{k_x,k_z} = -\sqrt{k_x^2\alpha_x^2 + k_z^2\alpha_z^2}\,\hat{u}_{k_x,k_z}. \tag{10}$$

In practice, the choice $y_{max} = 15$ has sufficed to yield numerical solutions with no discernible spurious boundary effects. Had zero perturbation boundary conditions been applied instead, a substantially larger value of y_{max} would have been required to yield comparable solutions.

An alternative to this domain truncation/asymptotic boundary condition approach is the use of a mapping from $\xi \in [0,1]$ to $y \in [0,\infty)$ --see Spalart (1986) and Laurien (1986). However, the present algorithm employs a staggered grid for the pressure, and for this alternative mapping it would require that matrix multiplies be used in place of Fast Fourier Transforms in several key locations in the code. As documented by Canuto, et al. (1988, Chapter 2), this would significantly increase the run time of the code, especially for simulations employing over 128 grid points in the normal direction. Moreover, the small value of y_{max} made possible by the use of asymptotic boundary conditions leads to the presence of relatively few grid points outside of the boundary layer.

Both the algebraic stretching

$$y = y_L \frac{1+\xi}{G-\xi} \qquad \xi = \frac{Gy-y_L}{y+y_L}$$

$$G = 1 + 2y_L/y_{max} \tag{11}$$

and the exponential stretching

$$y = -y_L \log(\frac{\xi-b}{a}) \qquad \xi = ae^{-y/y_L} + b$$

$$a = -2/[1 - e^{-y_{max}/y_L}] \tag{12}$$

$$b = [1 + e^{-y_{max}/y_L}][1 - e^{-y_{max}/y_L}]$$

were considered. The algebraic stretching is more robust for spectral algorithms: it yields spectral accuracy for solutions which decay only algebraically fast, as $y \to \infty$, whereas the exponential stretching requires exponential decay to achieve spectral accuracy (see Canuto, et al. (1988, Ch. 2)).

These mappings cluster the grid points near the wall. In the linear and early secondary instability stages the greatest need for resolution is near the wall and in the critical layer near $y = 0.6$ (in units of displacement thickness). However, as the tertiary instability develops, i.e., as the lambda vortex and detached shear layer intensify, additional resolution is required near the location of the shear layer, which rises toward the free stream as it breaks down. In these later stages of transition it is advantageous to compose the above mappings with a mapping from $\eta \in [-1,1]$ to $\xi \in [-1,1]$ which has the effect of clustering grid points near, say, $y = 3$. We have employed a hyperbolic tangent mapping of the form

$$\frac{\xi-\xi_0}{\Delta\xi} = \eta + \sigma \tanh \frac{\eta-\eta_0}{\Delta\eta}, \tag{13}$$

where ξ_0, $\Delta\xi$, η_0, $\Delta\eta$, and σ are chosen to provide the desired cluster-

ing. This combined mapping is readily accommodated witin the spectral collocation method.

The collocation grids ranged from 16 x 48 to 64 x 64 (in x and y) for the 2-D cases and from 16 x 48 x 8 to 64 x 64 x 16 (in x, y, and z) for the 3-D secondary instability studies. Typical simulations took several thousand time-steps and covered from two to five periods of the primary 2-D TS wave. The simulations of the tertiary instability took in excess of 10^6 total grid points. In all cases the grid was refined during the evolution of the instability so as to maintain a decrease of 8 orders of magnitude in the energy spectra in each coordinate direction (see Krist and Zang (1987)). The use of the additional mapping (13) enabled the tertiary instability simulations to be performed with less than half the points in y that would otherwise have been required.

A useful measure of the strength of a given Fourier harmonic is

$$E_{k_x,k_z}(t) = d_{k_x} d_{k_z} \int_0^{y_{max}} |\hat{u}_{k_x,k_z}(y,t)|^2 dy/E_0 \qquad (14)$$

where

$$d_k = 2 - \delta_{k0}.$$

This quantity is the kinetic energy of the mode normalized by the kinetic energy of the mean flow (E_0) between $y = 0$ and $y = y_{max}$. The constant d_k is used to account for the symmetries in the Fourier harmonics. Similarly, a measure of a given Chebyshev component is

$$E_n(t) = \int_0^{s_x L_x} \int_0^{s_z L_z} |\tilde{u}_n(x,z,t)|^2 dxdz \qquad (15)$$

$$/(s_x L_x s_z L_z E_0).$$

The accuracy of the fully non-linear, time-dependent Navier-Stokes code is documented in Table 1. For each of the linear modes specified in the first four columns, a highly accurate temporal eigenvalue ω and eigenfunction were generated using the Chebyshev tau code. This eigenfunction was then input at very low amplitude into the non-linear code as the inital condition. The code was run for two TS periods and the growth rate of the eigenfunction was measured. This is listed in the last column. Listed next to it is the growth rate (imaginary part of ω) produced by the linear stability code. This growth rate is effectively zero--the real part of ω is roughly 0.04. Keeping in mind the size of the real part of ω, it is clear from the table that the non-linear code is accurate to four or five digits.

Finite Amplitude Two-Dimensional Disturbances

Figure 6, taken from Lowell and Reshotko (1974), compares the neutral stability curves that ensue under heating control for $T_\infty = 60^\circ F$ when the temperature is allowed to fluctuate (solid lines) and when it is held fixed at its mean value (dashed lines). Note that the boundary layer is actually more stable than is suggested by linear theory calculations which neglect temperature fluctuations. Note also that although the flow initially becomes more stable as the wall is heated, its stability eventually degrades with additional wall heating. Lowell and Reshotko have performed further calculations in

which the effects of the temperature upon the density are included. They found that this effect moves the neutral stability curves to the left, e.g., for the $T_w = 90^oF$ case, the solid curve moves one-third of the distance to the dashed curve when density fluctuations are admitted.

The first set of results pertains to finite amplitude effects upon 2-D TS waves for a Re = 8950 boundary layer subjected to pressure gradient or heating control. The amount of control applied and the wavenumber of the least stable mode are included in Table 1. The control level was chosen to yield a growth rate of 0.0001 for the least stable 2-D TS wave. Results of simulations for which the initial amplitude of the 3-D wave was zero and the initial amplitude of the 2-D wave was 1/2, 1, 2, and 4% are summarized in Figure 7. Suction control yields behavior similar to that for pressure gradient control (Zang and Hussaini (1985b)) and is therefore not given. Two types of heating control simulations were performed: in one case the temperature was held fixed at its initial mean value (corresponding to the linear theory study of Wazzan, et al. (1968)), and in the other the temperature fluctuations were properly accounted for (as in the work of Lowell and Reshotko (1974)). The initial conditions for both types of heating simulations, however, were identical.

The strength of the perturbation at any instant is measured here by the kinetic energy $E_{1,0}(t)$ of the fundamental Fourier component of the velocity field. The ratio $E_{1,0}(t)/E_{1,0}(0)$ is plotted on a semi-log scale in Figure 7, with the time measured in units of the period of the 2-D TS wave. Thus, one indication of the impact of non-linear effects is the departure of the curves from a straight (and nearly horizontal) line. Another is the failure of the curves to lie on top of each other.

In all cases, the initial growth of the 2-D TS wave is faster than exponential. Note that in the non-linear regime the heated boundary layer appears to be less stable, i.e., subjected to faster growth of the 2-D wave, when temperature fluctuations are included. This is precisely the opposite of how temperature fluctuations affect the linear stability results. It is also apparent that non-linear effects lead to a more rapid destabilization of a water boundary layer controlled by heating than one controlled by pressure gradient. As will be shown below, it is the convection rather than the conduction terms in the temperature equation which are most responsible for this de-stabilization.

Tables 3 and 4 summarize the departure from linear growth for 2-D waves with initial amplitudes of 1/2% and 2%. The numbers give the ratios (after 1, 2, and 3 TS periods) of the actual amplitude of the 2-D wave to that given by linear theory. These numbers, of course, just reinforce the data presented in Figure 7.

Secondary Instability

The next part of this investigation focuses on finite amplitude effects upon the secondary instability of the primary 2-D wave to small, 3-D perturbations. The secondary instabilities may be categorized as fundamental or subharmonic. These are identified in flow visualizations of the early three-dimensional stage of transition as either ordered or staggered arrays of lambda vortices (Knapp and Roache (1968)), and have been explained by Floquet theory (Herbert (1984)). Figure 8 sketches the periodic array of vortices associated with these secondary instabilities. The distance L_x is the length of the primary 2-D TS wave.

The 3-D waves that lead to the fundamental instability are TS waves, i.e., solutions to the Orr-Sommerfeld equation, whereas the subharmonic instability arises from the interaction of the 2-D wave with a solution of the vertical vorticity (or Squire) equation with streamwise wavenumber $\alpha_x/2$. These so-called Squire modes are all linearly stable.

Figure 9 summarizes the results of numerical simulations of the secondary instability of controlled boundary layers under the same $Re = 8950$ conditions used for the 2-D simulations. The initial phases of the 3-D TS wave and the Squire waves were, respectively, 39^o behind and 4^0 behind the 2-D TS wave for the pressure gradient case. For the heated cases, the 3-D wave was 45^o behind and the Squire wave 7^o ahead. The phase of each wave is judged by the location of the maximum in the streamwise velocity perturbation. In all cases, the initial 3-D amplitude was 0.01% and the initial 2-D amplitude varied between 1/2% and 4%. In these plots, the kinetic energy is shown for the 2-D Fourier component $(k_x,k_z) = (1,0)$ and for the appropriate 3-D component--(1,1) for the fundamental instability and (1/2,1) for the subharmonic. The 3-D curves are labeled by the amplitude of the 2-D wave for the simulation.

The secondary instabilities have the same general character here that they do in uncontrolled boundary layers: they are triggered by 2-D amplitudes on the order of 1% or more; their growth rate increases with the 2-D amplitude; they grow much faster than the primary wave; and the fundamental and subharmonic instabilities have comparable growth rates.

Among these three cases, the secondary instability is strongest for the heated boundary layer simulation which includes temperature fluctuations. But the more rapid growth of the 3-D waves in this case is clearly tied to the

more rapid growth of the 2-D wave. Hence, the principal effect of the temperature fluctuations is upon the 2-D waves.

Towards the Tertiary Instability

We now seek to determine the effect of LFC techniques on the formation of the lambda vortex and of the detached shear layer whose roll-up into hairpin eddies is believed responsible for the tertiary instability. Our comparisons will be made with the Re = 1100 experiment of Kovasznay, Komoda, and Vasudeva (1962), referred to hereafter as KKV, in which detailed measurments were made of the detached shear layer resulting from a fundamental mode transition. The basic parameters of the simulations are listed in Table 5. The magnitudes of the pressure gradient and heating controls were chosen so that each provides a 7% decay in the amplitude of the velocity fluctuation of the 2-D TS wave in a single period. The controls here are so weak that the TS period of the heated case is only 2% longer than those of the uncontolled and pressure gradient cases.

Clearly, the secondary instability exists for the uncontrolled case, regardless of the initial amplitude of the unstable 2-D wave, because the 2-D wave will eventually grow sufficiently large to trigger the explosive growth of 3-D waves. A parametric study of the controlled cases reveals that the threshold initial 2-D amplitude for the onset of the secondary instability is approximately 1.5% for both pressure gradient and (fixed temperature) heating control.

The initial amplitudes used by Wray and Hussaini (1984) in their numerical simulation of the KKV experiment were $\varepsilon_2 = 0.018$ and $\varepsilon_3 = .008$. These

have been adopted in the present repeat of their simulation of the uncontrolled case. At $t = 0$ the 3-D wave is 36° behind the 2-D wave. A time history of the low-order Fourier components of this case is shown in Figure 10. Both the 2-D and 3-D TS waves (labeled (1,0) and (1,1) respectively in the figure) are linearly unstable. The 2-D TS wave grows at nearly its linear rate for more than 3 periods. The 3-D TS wave initially grows at its linear rate, but shortly commences a far more rapid growth due to the secondary instability. Before the end of the fourth TS period the flow is strongly three-dimensional, as evidenced here by the presence of Fourier harmonics--(1,1) and (0,2)--which have larger amplitudes than the primary 2-D waves.

This figure also furnishes a comparison with two controlled cases, one with pressure gradient and another with heating. In the latter simulation, temperature fluctuations were excluded. The 3-D waves were 40° behind the 2-D waves in both cases. For each controlled flow, both TS waves are linearly damped. The secondary instability is evident, although it is substantially weaker than it is for the uncontrolled boundary layer. Indeed, it is not until the seventh TS period that the controlled flows became predominantly three-dimensional. The reduced strength of the secondary instability is due partly to the improved stability of the controlled mean flow profile and partly to the decay of the 2-D TS waves. After 1 period, the uncontrolled 2-D TS wave has an amplitude of 2.3%, compared with the 1.7% amplitude of the controlled cases at the same time.

The maximum perturbations occur in the so-called "peak plane," which is the symmetry plane (in the spanwise direction). The improvement produced by the LFC techniques is emphasized by the plots of vertical shear in the peak plane after roughly four periods (Figure 11). The detached shear layer in the

uncontrolled case is quite distinct and already has the sharp kink characteristic of the "one-spike" stage (KKV). The controlled flows are still so early in the transition process that the detached shear layer has not yet developed.

Another set of simulations has been performed to illustrate the effect of temperature fluctuations. The example for this comparison will be the same as the previous case except that $\varepsilon_2 = 0.027$ instead of 0.018. The increased amplitude of the primary wave permits the strong detached shear layer to form by $t = 4$ in the controlled cases. The results are given in Figure 12 and include calculations for $Pr = 1$ as well as $Pr = 7.0$.

In all three cases shown in Figure 12, the flow becomes predominantly three-dimensional during the fourth TS period. (In the uncontrolled case with $\varepsilon_2 = .027$, this occurs during the third period.) The larger 2-D amplitude of the initial conditions for the present cases compensates for the enhanced stability of their mean flow profiles.

Notice once again that temperature perturbations have a substantial, destabilizing effect. This is especially so for the realistic case with $Pr = 7$. The comparison case with $Pr = 1$ has a higher conductivity and thus has faster damping of temperature fluctuations. Apparently the destabilizing effects of the temperature fluctuations are due to convection, since the flow is more stable as the conductivity is increased. Figure 13 illustrates the differences in the formation of the detached shear layers in these cases.

The characteristic lambda vortex and detached shear layer structures of the K-type transition have been documented experimentally by Williams, Fasel, and Hama (1984) for an uncontrolled boundary layer. Detailed mappings of it have been provided by Krist and Zang (1987) in their numerical simulations of both sub-critical and super-critical channel flow transitions. Here we focus

on relating the temperature fluctuations to the lambda vortex and the detached shear layer.

Figures 14 and 15 illustrate the flow fields which develop at an advanced stage of the fundamental secondary instability in an uncontrolled and a heated boundary layer. The former case had an initial 2-D amplitude of 1.8% and is shown in Figure 14 at $t = 3\frac{7}{8}$ from a calculation on a 96 x 96 x 192 grid. The initial 2-D amplitude of the heated case was 2.7%; it is shown in Figure 15 at $t = 4\frac{1}{4}$ and the grid was 96 x 162 x 216. The flat plate is indicated by the solid surface and the mean flow is from the lower right to the upper left. The peak plane is located in the middle of the spanwise direction in these figures.

The flow field is particularly clear in the case of the uncontrolled boundary layer. The vortex lines in Figure 14 indicate the presence of a lambda vortex suggest the emergence of a hairpin eddy at the vortex tip, and demonstrate the existence of the inverted vortex which has been observed experimentally (Williams (1987)). The inverted vortex is a structure characterized by vortex lines which bend upstream and down towards the wall. It is located in the vicinity of the critical layer about a third of a wavelength upstream of the tip of the principal vortex, and just underneath the start of the detached shear layer. Zang, Krist, Erlebacher, and Hussaini (1987) have discussed the physical origin of this structure in transitional flows. The spanwise vorticity displays the strong detached shear layer which forms on top of the vortex. The normal velocity contours indicate the regions in which low speed fluid from the wall region is ejected upward towards the free stream. The peak plane is located at the center of the hairpin vortex. In this plane, the detached shear layer is strongest and the upward normal velocity is most intense.

The flow field of the heated case is quite similar, although the lambda vortices and detached shear layers are less intense in this more stable flow. Of special interest in Figure 15 are the contours of the temperature perturbation. They represent the local departure from the mean temperature. Note that the temperature fluctuations are strongly correlated with the normal velocity. There is a temperature increase in the peak plane, where hot fluid is convected upwards, and an even stronger temperature decrease near the wall on the outer regions of the legs of the lambda vortex, where cold fluid is convected downwards.

Williams introduced a finite amplitude 2-D TS wave by means of a vibrating ribbon and let the three-dimensional structure develop from random perturbations in the flow. The present numerical simulation used regular, non-noisy initial conditions in the form of a 2-D TS wave and two oblique 3-D waves. Thus, the flow-field structures in the simulations are more regular and yield finer detail on the dynamics of the lambda vortex and the detached shear layer.

The Role of Longitudinal Vortices

Several recent experiments on the control of boundary-layer transition have resorted to the principle of wave superposition to delay transition. They have employed either a vibrating ribbon (Milling (1981), Thomas (1983)) or else a heating element (Liepmann, Brown, and Nosenchuck (1982)) to introduce a 2-D TS wave, and a second control element some distance downstream of the first to introduce a second 2-D TS wave which was tuned in amplitude and phase to cancel out as much of the evolved TS wave as possible. The delay in

transition occurred because the reduced amplitude of the 2-D TS wave resulted in a decreased strength of the nonlinear instabilities which lead to transition.

Liepmann and Nosenchuck (1982) have implemented a feedback control mechanism to drive their second heating element. Their sensor was able to detect both 2-D TS waves deliberately excited by an upstream heating element and naturally occurring 2-D TS waves. They demonstrated that both artificial and natural transition can be delayed by such a control mechanism.

Several numerical experiments, for example, by Kleiser and Laurien (1984), and Laurien (1986), have simulated LFC wave superposition produced by suction. These results are similar to those of the experiments described above.

Both the experiments and the simulation have focused on the control of the 2-D TS wave. The secondary instability involves other waves as well, notably the two oblique 3-D TS waves and the spanwise mode $(k_x,k_z) = (0,1)$. The simplest and apparently the strongest secondary instability mechanism involves the (1,0), (1,1) + (1,-1), and (0,1) modes. The 2-D TS wave is by far the most energetic of these. But the possibility exists that control of one of the remaining modes might prove equally effective in delaying transition.

Zang and Hussaini (1985a) demonstrated that control of the spanwise mode did indeed delay transition. This demonstration consisted of a series of numerical simulations in which the usual initial conditions were employed, but in which the (0,1) mode was artificially and completely suppressed at each time step. This artifice is not completely physically realizable, of course, but it is a first step in analyzing the effectiveness of spanwise mode suppression.

Most of the numerical simulations reported there were for channel flow. The results indicated that at low Reynolds number, i.e., 1500, spanwise mode suppression eliminates the subcritical, secondary instability, and at higher Reynolds numbers, e.g., 5000, this instability is substantially reduced. Similar results were obtained for the uniformly controlled parallel boundary layer at the low Reynolds number of 518 and at the higher one of 8950.

An example of these results is shown here in Figure 16 for the heated boundary layer at $Re = 1100$, where, for simplicity, the temperature is held fixed at its mean level. At a 2-D TS wave amplitude of 2.7%, control of the spanwise mode is not sufficient to stabilize the flow. However, the remaining instability is quite weak and no longer has the character of the lambda vortex and detached shear layer. Even after 8 TS periods the original oblique modes are still of lower amplitude than the 2-D mode. The flow field at $t = 8$ is illustrated in Figure 17. (The grid here was $36 \times 96 \times 192$.) The vortex lines are only mildly distorted and there is no indication of a lambda vortex. There is a pair of counterrotating longitudinal vortices pinched close together near the peak plane. However, as is documented in Table 6, the intensity of this instability is far less than when the spanwise mode is operational.

Concluding Remarks

For all of the LFC techniques examined here, finite amplitude effects are destabilizing, i.e., finite amplitude 2-D TS waves grow faster than predicted by linear theory. We also find, in direct contrast to the results from linear theory for low amplitude waves, that temperature fluctuations exert a further

de-stabilizing influence on finite amplitude 2-D TS waves. The controlled boundary layers are, of course, subject to intense 3-D secondary instabilities. The instantaneous growth rates of both the fundamental and subharmonic instabilities are strongly tied to the amplitude of the primary 2-D wave. The principal finite amplitude effects upon the 3-D secondary instabilities occur through the faster growth of the 2-D wave.

The secondary instabilities of flows controlled by uniform pressure gradient, suction, and heating are qualitatively similar to each other and to uncontrolled flows. The principal quantitative difference is between wall-heated boundary layers and the other two controlled cases. Especially when one translates the parallel boundary layer results into terms appropriate for the growing boundary layer, our numerical results indicate that the nonlinear instabilities of heated flows are more severe than those of flows controlled equally well in a linear sense by pressure gradient or suction.

The pronounced effect of temperature perturbations in heated boundary layers is responsible for part of this difference. Flow-field analysis of the heated boundary-layer simulation reveals that the temperature fluctuations are largely due to convection driven by the temperature gradients.

The investigation of spanwise mode control has disclosed that this can substantially delay transition. It also has suggested that several different nonlinear interactions contribute significantly to the secondary instability.

Acknowledgment

Research was supported by the National Aeronautics and Space Administration under NASA Contract NAS1-17070 while the second author was in residence at ICASE, NASA Langley Research Center, Hampton, VA 23665.

References

Barker, S. J. (1979): Twelfth Symposium on Naval Hydrodynamics, p. 77.

Benney, D. J.; and Lin, C. C. (1960): On the Secondary Motion Induced by Oscillation in a Shear Flow. Phys. Fluids, Vol. 3, pp. 656-657.

Canuto, C.; Hussaini, M. Y.; Quarteroni, A.; and Zang, T. A. (1988): Spectral Methods in Fluid Dynamics, Springer-Verlag, Berlin.

Gilbert, N.; and Kleiser, L. (1986): Subcritical transition to turbulence in channel flow, in Direct and Large Eddy Simulation of Turbulence, U. Schumann and R. Friedrich (eds.), Vieweg, Braunschweig, pp. 1-18.

Hama, F. R.; and Nutant, J. (1963): Detailed Flow-Field Observations in the Transition Process in a Thick Boundary Layer. Proc. of the 1963 Heat Transfer and Fluid Mechanics Institute, Stanford Univ. Press, Palo Alto, pp. 77-93.

Hefner, J. N; and Bushnell, D. M. (1979): Application of Stability Theory to Laminar Flow Control. AIAA Paper 79-1493.

Herbert, T. (1983): Secondary Instability of Plane Channel Flow to Subharmonic Three-Dimensional Disturbances. Phys. Fl., Vol. 26, pp. 871-874.

Herbert, T. (1984): Analysis of the Subharmonic Route to Transition in Boundary Layers, AIAA Paper No. 84-0009.

Herbert, T. (1988): Secondary Instability of Boundary Layers. Ann. Rev. Fl. Mech., Vol. 20, pp. 487-526.

Klebanoff, P. S.; Tidstrom, K. D.; and Sargent, L. M. (1962): The Three-Dimensional Nature of Boundary-Layer Instability. J. Fl. Mech., Vol. 12, pp. 1-34.

Kleiser, L.; and Laurien, E. (1984): Three-Dimensional Numerical Simulation of Laminar-Turbulent Transition and its Control by Periodic Disturbances. Proc. 2nd IUTAM Symposium on Laminar-Turbulent Transition. Springer-Verlag, Berlin.

Kleiser, L.; and Schumann, U. (1984): Spectral Simulation of the Laminar-Turbulent Transition Process in Plane Poiseuille Flow. Spectral Methods for Partial Differential Equations (R. G. Voigt, D. Gottlieb, and M. Y. Hussaini, eds.), SIAM-CBMS, Philadelphia, pp. 141-163.

Knapp, C. F.; and Roache, P. J. (1968): A Combined Visual and Hot-wire Anemometer Investigation of Boundary-Layer Transition, AIAA J., Vol. 6, pp. 29-36.

Kovasznay, L. S.; Komoda, H.; and Vasudeva, B. R. (1962): Proc. 1962 Heat Transfer and Fluid Mechanics Institute, Stanford Univ. Press, Palo Alto, pp. 1-26.

Krist, S. E.; and Zang, T. A. (1987): Numerical Simulation of Channel Flow Transition. NASA TP 2667.

Laurien, E. (1986): Numerische Simulation zur Aktiven Beeinflussung des Laminar-Turbulenten Ubergangs in der Plattengrenzschichtströmung, DFVLR-FB 86-5.

Liepmann, H. W.; Brown, G. L.; and Nosenchuck, D. M. (1982): Control of Laminar-Instability Waves Using a New Technique, J. Fl. Mech., Vol. 118, pp. 187-200.

Liepmann, H. W.; and Nosenchuck, D. M. (1982): Active Control of Laminar-Turbulent Transition, J. Fl. Mech., Vol. 118, pp. 201-204.

Lowell, R. L.; and Reshotko, E. (1974): Numerical Study of a Heated Water Boundary Layer, Report FT AS/TR-73-93, Case Western Reserve University.

Malik, M. R.; Chuang, S.; and Hussaini, M. Y. (1982): Accurate Numerical Solution of Compressible Stability Equations, ZAMP, Vol. 33, pp. 189-201.

Malik, M. R.; Zang, T. A.; and Hussaini, M. Y. (1985): A Spectral Collocation Method for the Navier-Stokes Equations, J. Comput. Phys., Vol. 61, pp. 64-88.

Milling, R. W. (1981): Tollmien-Schlichting Wave Cancellation. Phys. Fluids, Vol. 24, pp. 979-981.

Morkovin, M. V. (1969): On the Many Faces of Transition. Viscous Drag Reduction, (C. S. Wells, ed.), Plenum Press, New York, pp. 1-31.

Orszag, S. A. (1971): Accurate Solution of the Orr-Sommerfeld Stability Equation, J. Fl. Mech., Vol. 50, pp. 689-703.

Orszag, S. A.; and Patera, A. T. (1983): Secondary Instability of Wall-Bounded Shear Flows. J. Fl. Mech., Vol. 128, pp. 347-385.

Spalart, P. R. (1986): Numerical Simulation of Boundary Layers. Part 1. Weak Formulation and Numerical Method. NASA TM-88222.

Spalart, P. R.; and Yang, K. S. (1987): Numerical Simulation of Ribbon-Induced Transition in Blasius Flow. J. Fl. Mech., Vol. 178, pp. 345-365.

Strazisar, A. J.; Reshotko, E.; and Prahl, J. M. (1977): Experimental Study of the Stability of Heated Laminar Boundary Layers in Water. J. Fl. Mech., Vol. 83, pp. 225-247.

Thomas, A. S. W. (1983): The Control of Boundary-Layer Transition Using a Wave-Superposition Principle. J. Fl. Mech., Vol. 137, pp. 223-250.

Wazzan, A. R.; Okamura, T.; and Smith, A. M. O. (1968): The Stability of Water Flow Over Heated and Cooled Flat Plates. J. of Heat Transfer, Vol. 90, pp. 109-114.

Williams, D. R. (1987): Vortical Structures in the Breakdown Stage of Transition. Stability of Time Dependent and Spatially Varying Flows, D. L. Dwoyer and M. Y. Hussaini (eds.), Springer, New York, pp. 335-350.

Williams, D. R.; Fasel, H.; and Hama, F. R. (1984): Experimental Determination of the Three-Dimensional Vorticity Field in the Boundary-Layer Transition Process. J. Fl. Mech., Vol. 149, pp. 179-203.

Wortmann, F. X. (1977): The Incompressible Fluid Motion Downstream of Two-Dimensional Tollmien-Schlichting Waves, in Laminar-Turbulent Transition, AGARD CP-224, pp. 12/1-8.

Wray, A.; Hussaini, M. Y.; and Degani, D. (1977): Numerical Simulation of Transition to Turbulence. Proc. 2nd GAMM Conference on Numerical Methods in Fluid Dynamics, Vieweg, Braunschweig.

Wray, A.; and Hussaini, M. Y. (1980): Numerical Experiments in Boundary-Layer Stability, AIAA Paper 80-0275.

Wray, A.; and Hussaini, M. Y. (1984): Numerical Experiments in Boundary-Layer Stability. Proc. Roy. Soc. London A., Vol. 392, pp. 373-389.

Zang, T. A. (1988): On the Rotation and Skew-Symmetric Forms for Incompressible Flow Simulations, Appl. Numer. Math., to appear.

Zang, T. A.; and Hussaini, M. Y. (1985a): Numerical Experiments on Subcritical Transition Mechanisms. AIAA Paper 85-0296.

Zang, T. A.; and Hussaini, M. Y. (1985b): Numerical Experiments on the Stability of Controlled Shear Flows. AIAA Paper No. 85-1698.

Zang, T. A.; and Hussaini, M. Y. (1986): On Spectral Multigrid Methods for the Time-Dependent Navier-Stokes Equations. Appl. Math. Comp., Vol. 19, pp. 359-372.

Zang, T. A.; Krist, S. E.; Erlebacher, G.; and Hussaini, M. Y.: Nonlinear Structures in the Later Stages of Transition. AIAA Paper No. 87-1204.

Table 1. Some Controlled Boundary-Layer Modes for Re = 8950

Control	Mode	α	β	ω_r	ω_i	$\omega_{i\|calc}$
$\beta_p = 0.55$	TS 2-D	0.167675	0.00	0.037384	0.000095	0.000096
	TS 3-D	0.167675	0.167675	0.040948	-0.001012	-0.001028
$F_w = 0.895$	TS 2-D	0.162057	0.00	0.036207	0.000093	0.000093
	TS 3-D	0.162057	0.162057	0.039742	-0.000968	-0.000993
$\tau = 1.10$	TS 2-D	0.149937	0.00	0.029337	0.000093	0.000097
	TS 3-D	0.149937	0.149937	0.032105	-0.000798	-0.000793

Table 2. Mean Flow Characteristics for Re = 8950

Control	$\delta^*/\sqrt{\frac{\nu x_0}{u_\infty}}$	Re_{δ^*} Blasius
None	1.7244	8,950
$\beta = 0.55$	0.9448	16,330
$\tau = 1.10$	1.3986	11,040

Table 3. Non-linear/Linear Amplitude Ratio for 1/2% 2-D Waves

TIME	PRESSURE GRADIENT	HEATING (FIXED T)	HEATING
1	1.004	1.005	1.001
2	1.013	1.017	1.016
3	1.022	1.030	1.080

Table 4. Non-linear/Linear Amplitude Ratio for 2% 2-D Waves

TIME	PRESSURE GRADIENT	HEATING (FIXED T)	HEATING
1	1.050	1.065	1.184
2	1.189	1.257	1.605
3	1.378	1.567	2.387

Table 5. Some Controlled Boundary-Layer Modes for Re = 1100

Control	Mode	α	β	ω_r	ω_i
none	TS 2-D	.250	0.	.08624	.00333
	TS 3-D	.250	.209	.09396	.00126
β_p = .1054	TS 2-D	.250	0.	.08662	-.00100
	TS 3-D	.250	.209	.09349	-.00307
τ = 1.0275	TS 2-D	.250	0.	.08486	-.00102
	TS 3-D	.250	.209	.09161	-.00372

Table 6. Effect of Spanwise Mode on Transition

Case	$\varepsilon_2(t=0)$	t	$\omega_x\|_{max}$	$\omega_z\|_{max}$	$v\|_{max}$
uncontrolled	0.018	3 7/8	1.6	1.5	0.20
heated	0.027	4 1/4	1.2	1.0	0.085
heated (spanwise mode suppressed)	0.027	8	0.4	0.8	0.034

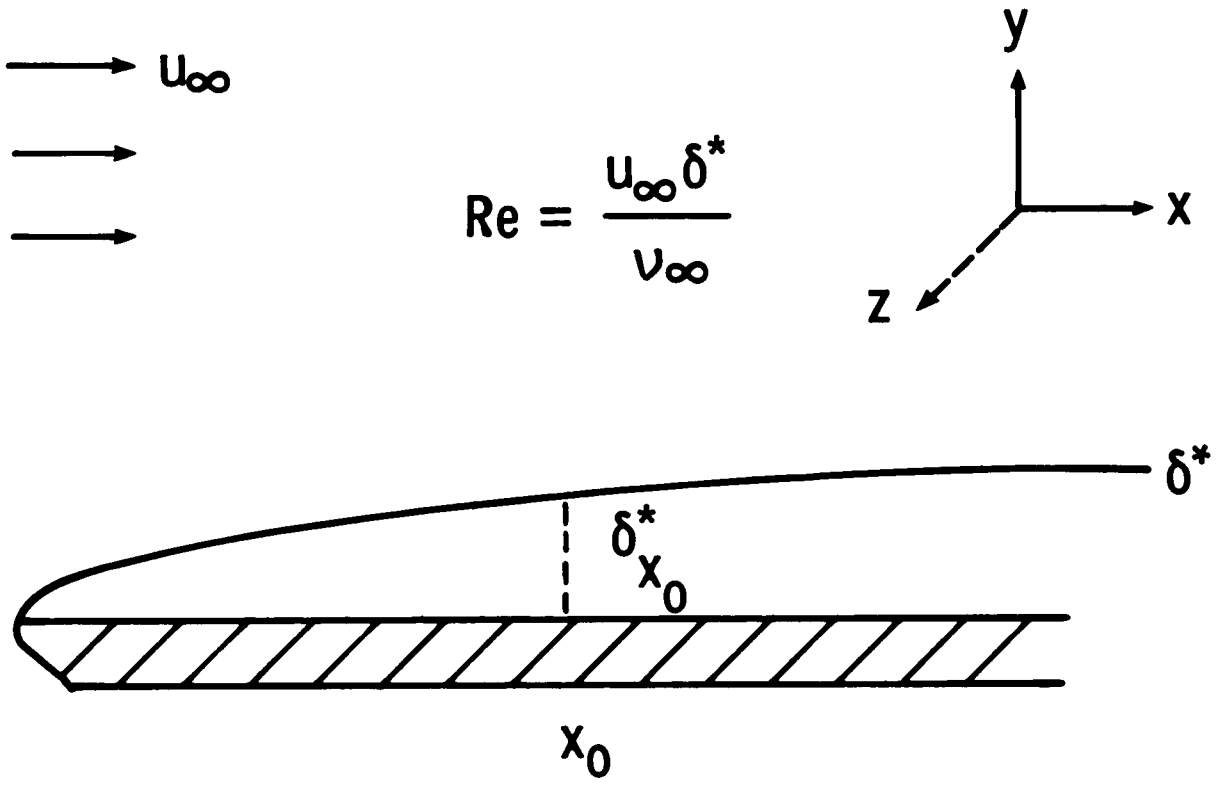

Fig. 1. Schematic of the growing boundary layer on a flat plate.

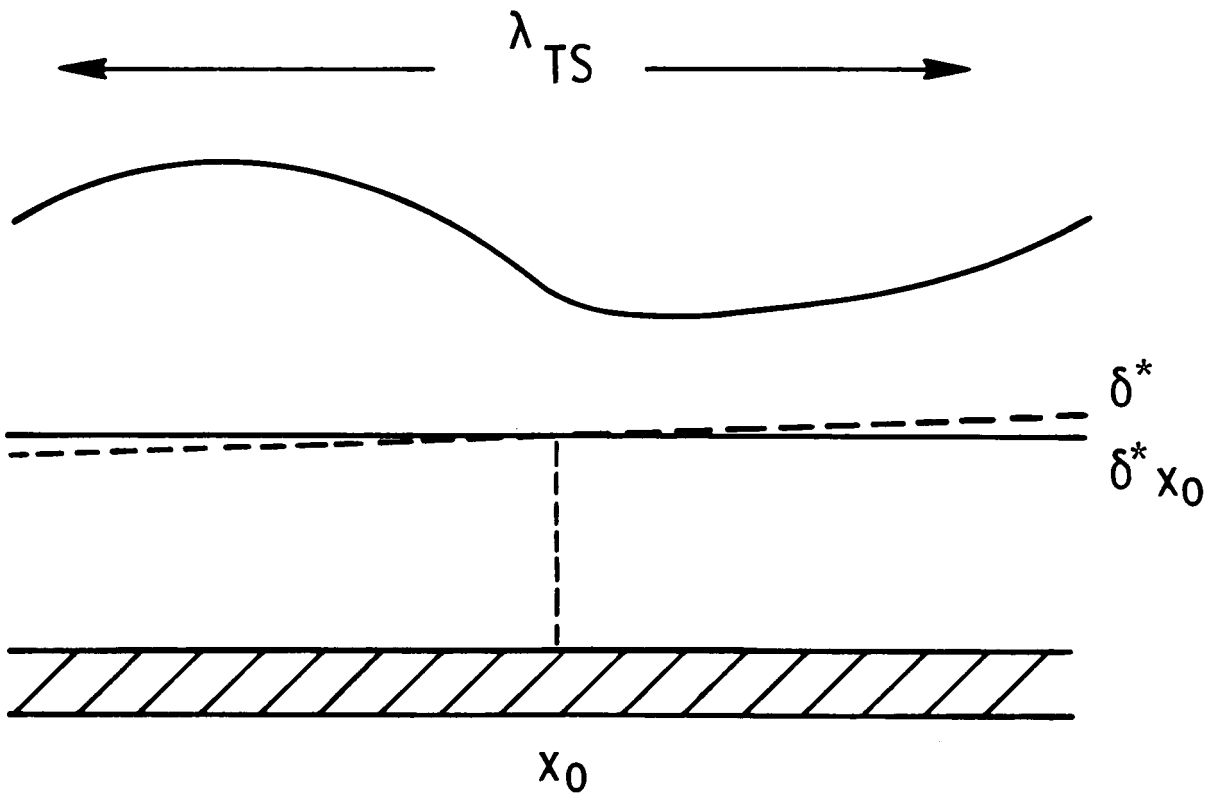

Fig. 2. Schematic of the parallel boundary layer approximation.

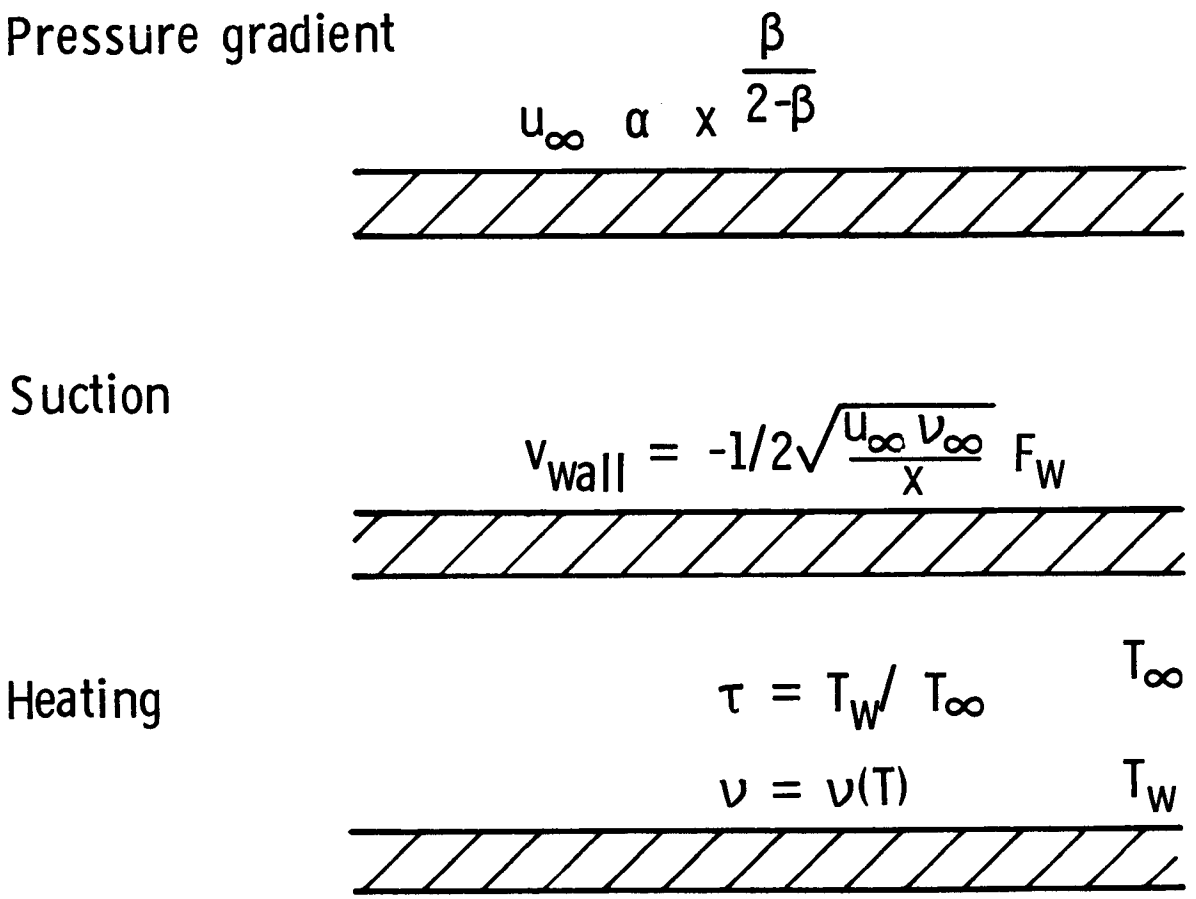

Fig. 3. Definition of laminar flow control parameters.

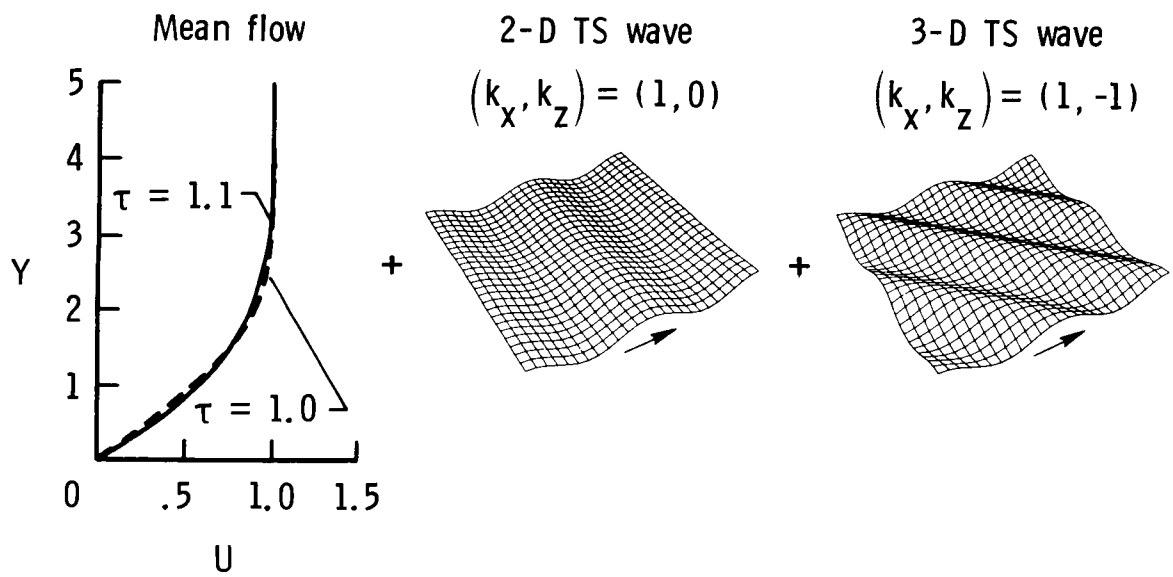

Fig. 4. Initial conditions for 3-D numerical simulations.

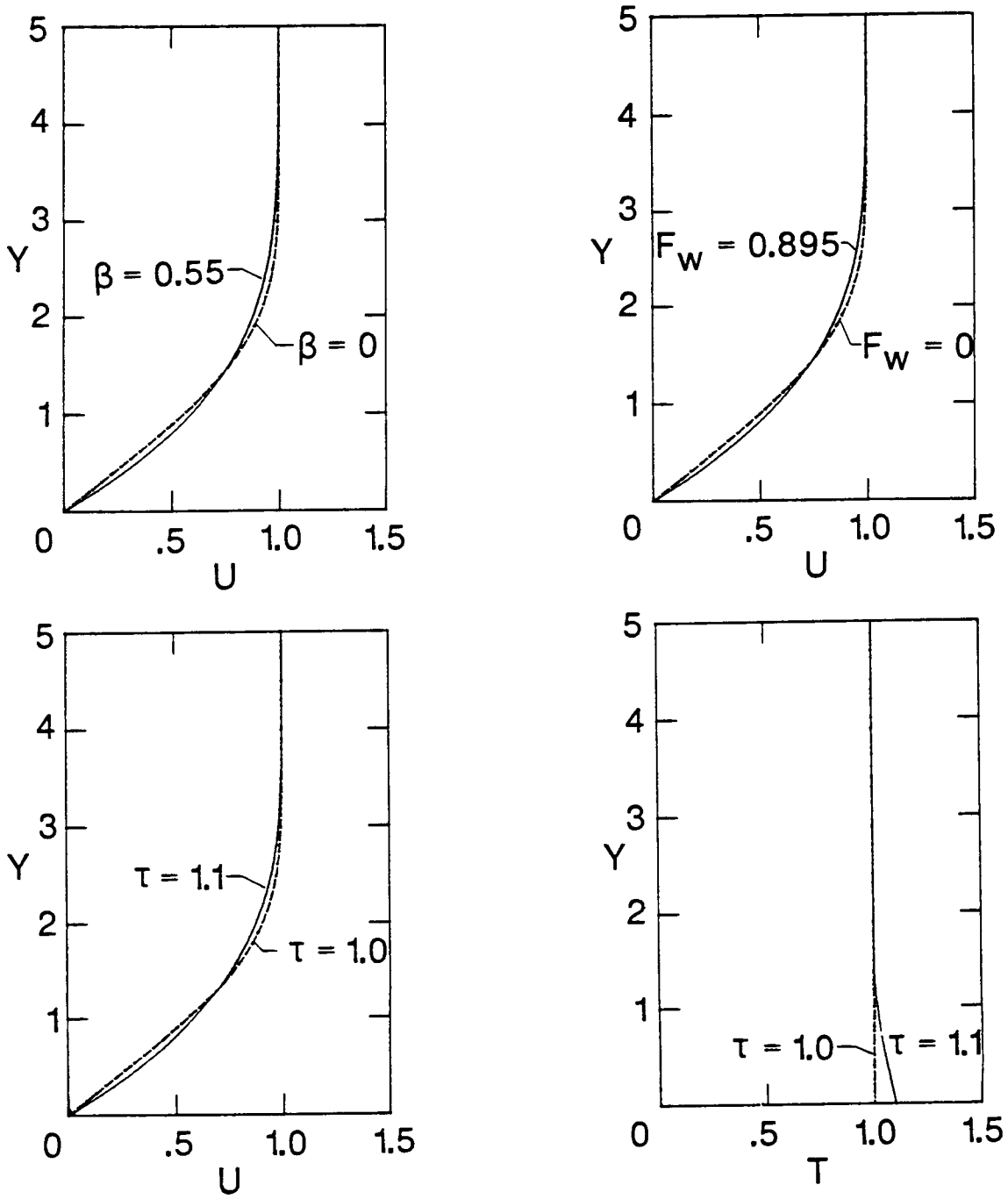

Fig. 5. Mean flow profiles at Re = 8950. The velocity U and temperature T are scaled by their freestream values. The normal coordinate y is scaled by the displacement thickness. The uncontrolled profiles are indicated by the dashed line.

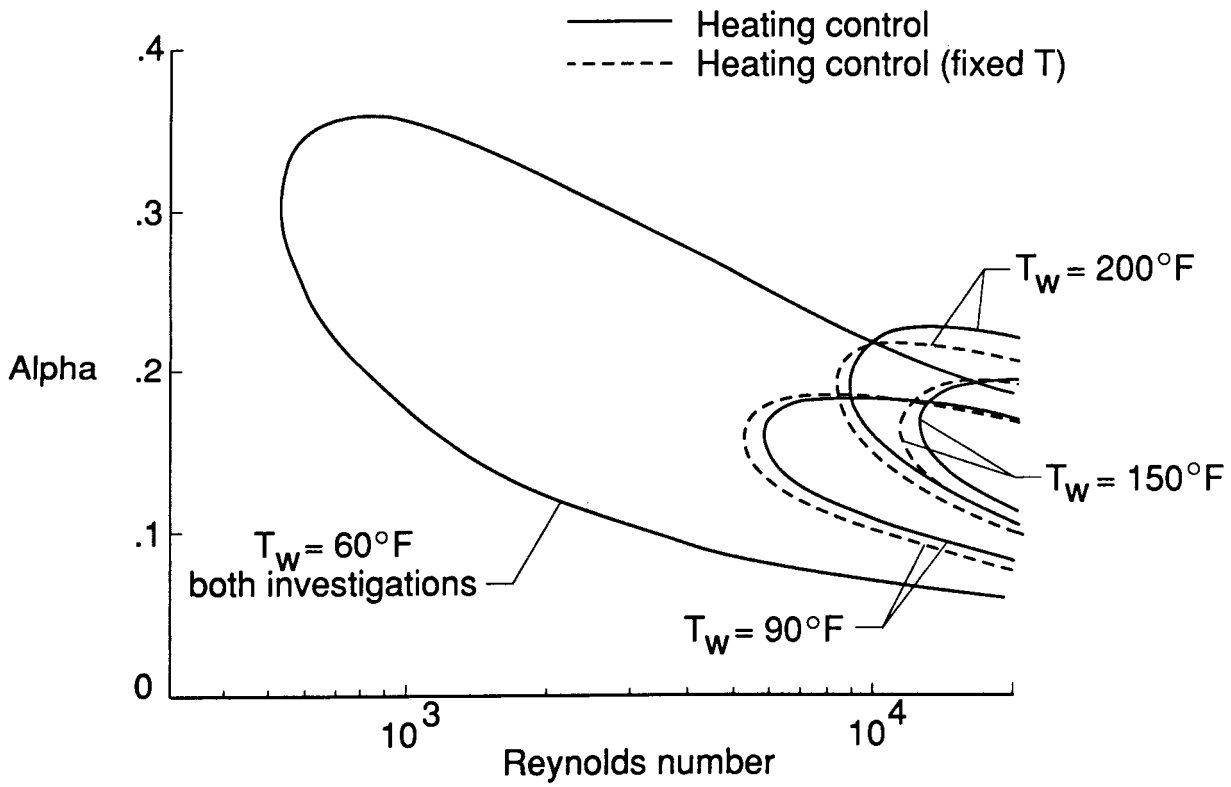

Fig. 6. Neutral curves for heated boundary layers (Lowell and Reshotko (1974)).

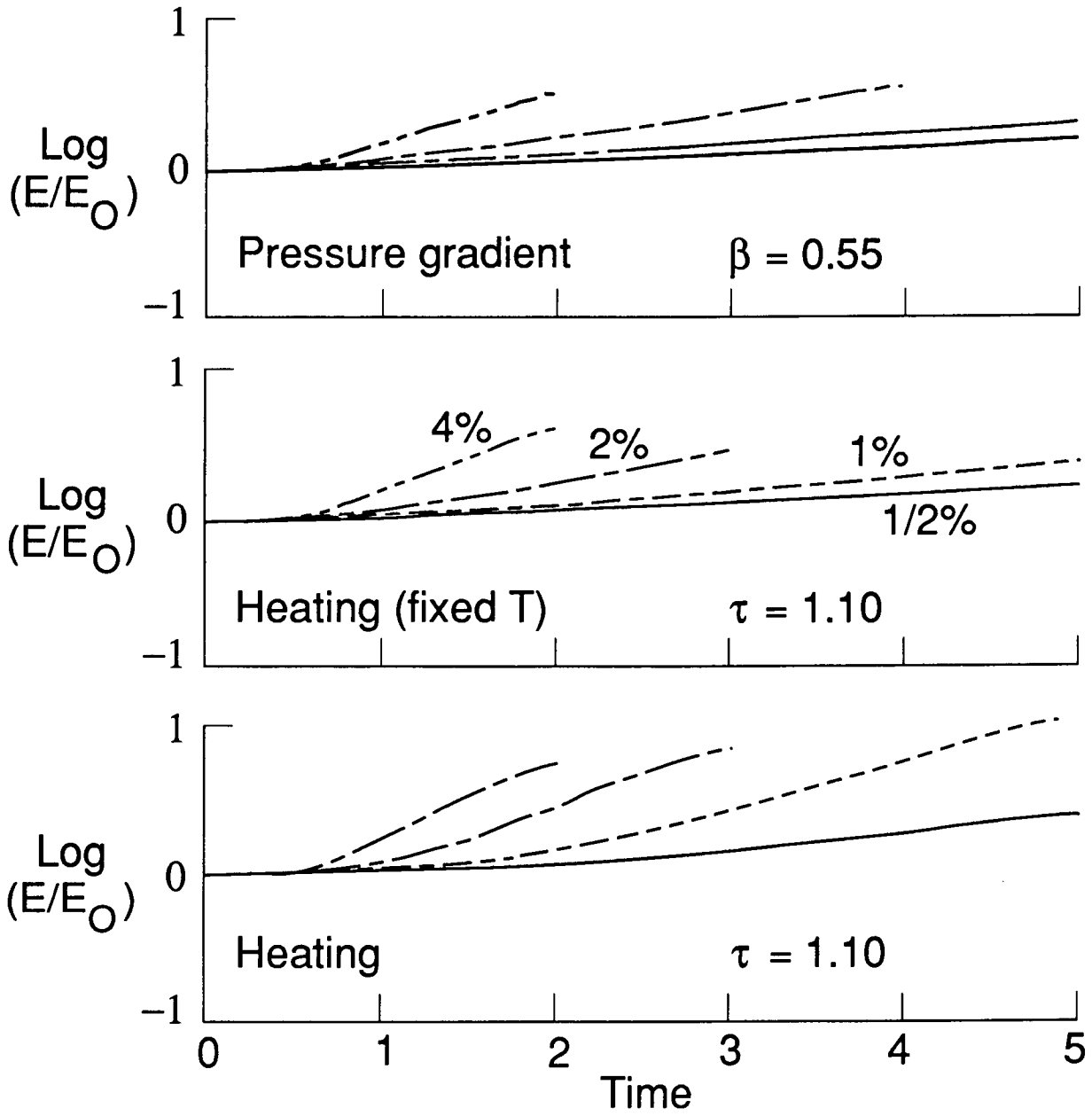

Fig. 7. Growth of finite amplitude 2-D TS waves at Re = 8950. Time is measured in units of the period of the uncontrolled two-dimensional TS wave.

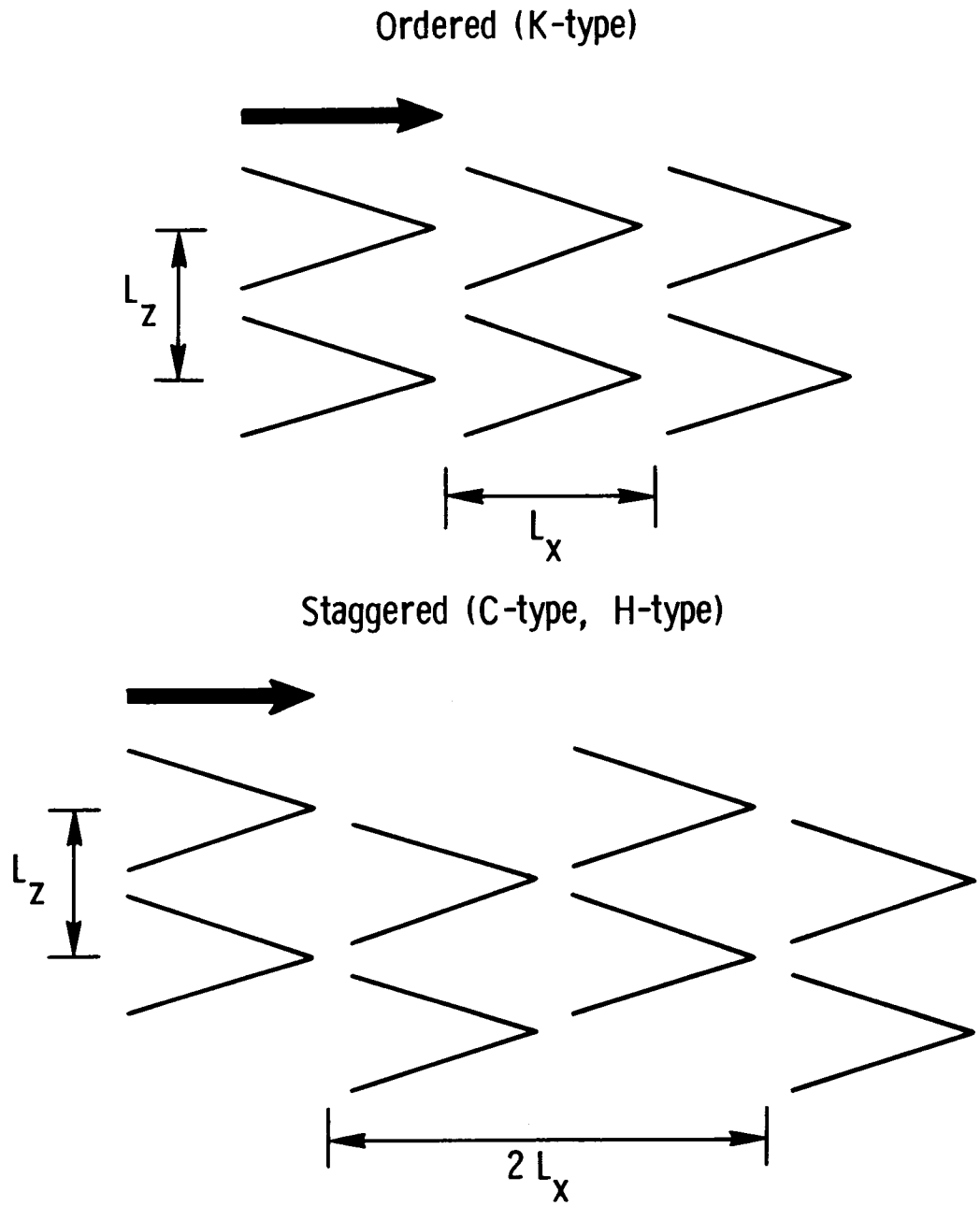

Fig. 8. Schematic of lambda vortex patterns arising from secondary instabilities.

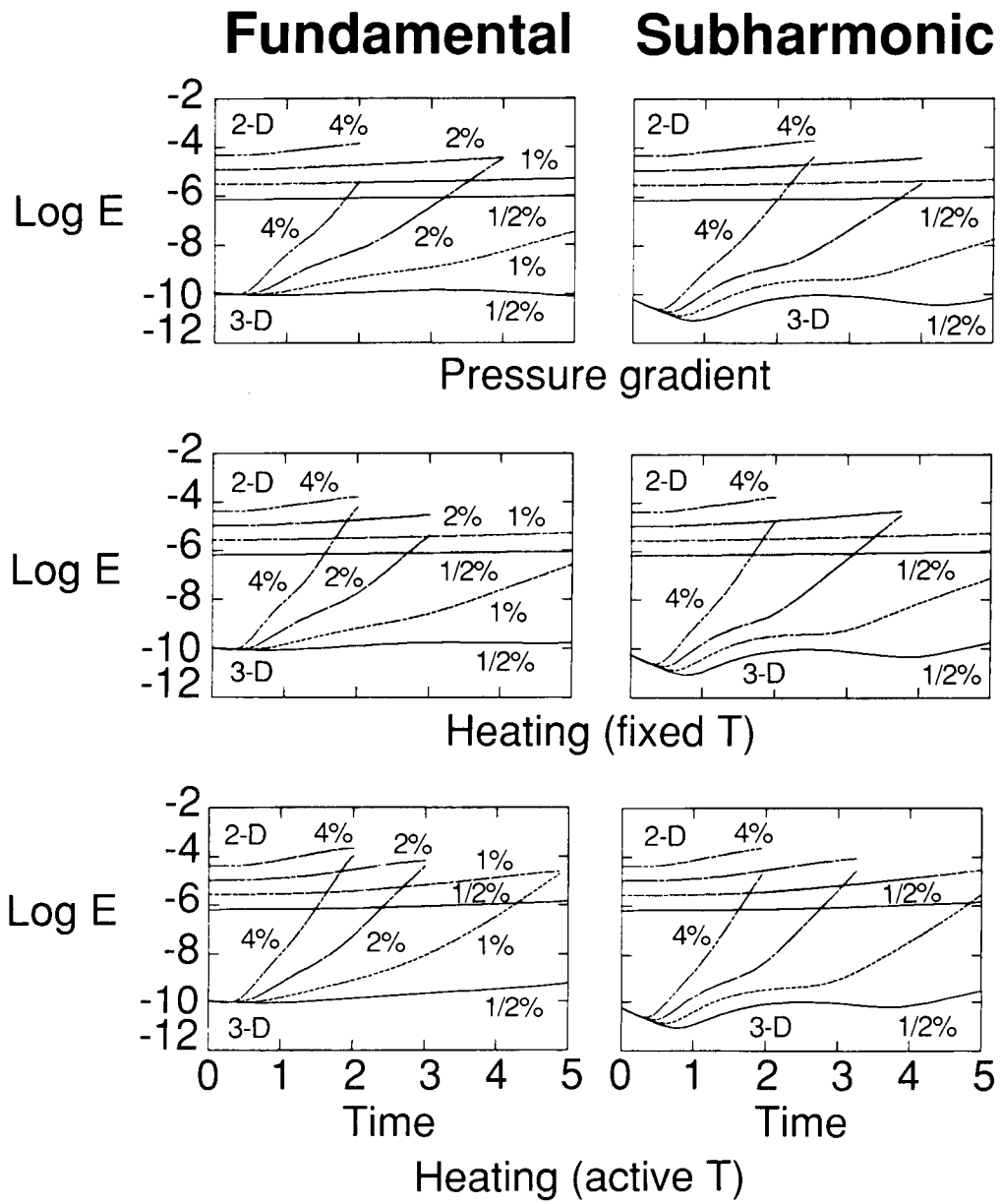

Fig. 9. Secondary instability of controlled boundary layers at Re = 8950.

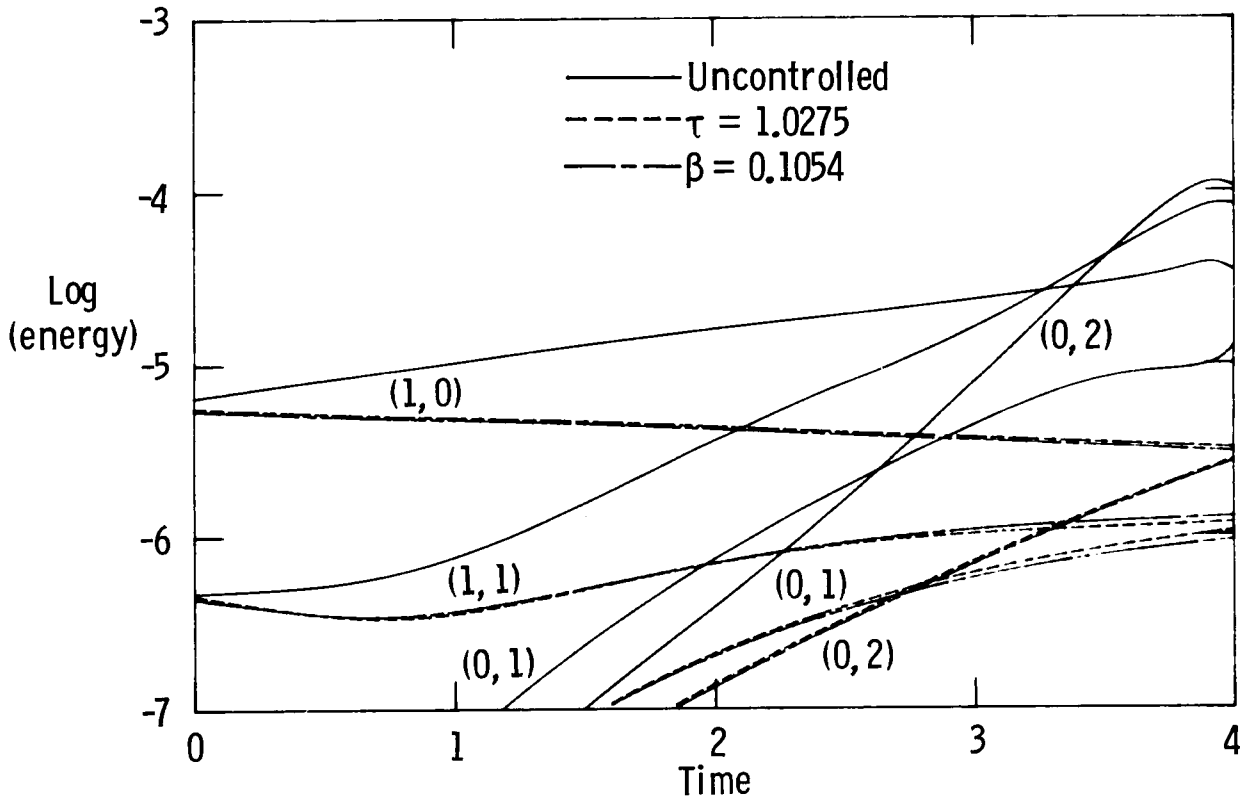

Fig. 10. Harmonic history for Re = 1100 boundary layer simulations starting with a 1.8% two-dimensional TS wave and a 0.8% combination of two three-dimensional TS waves.

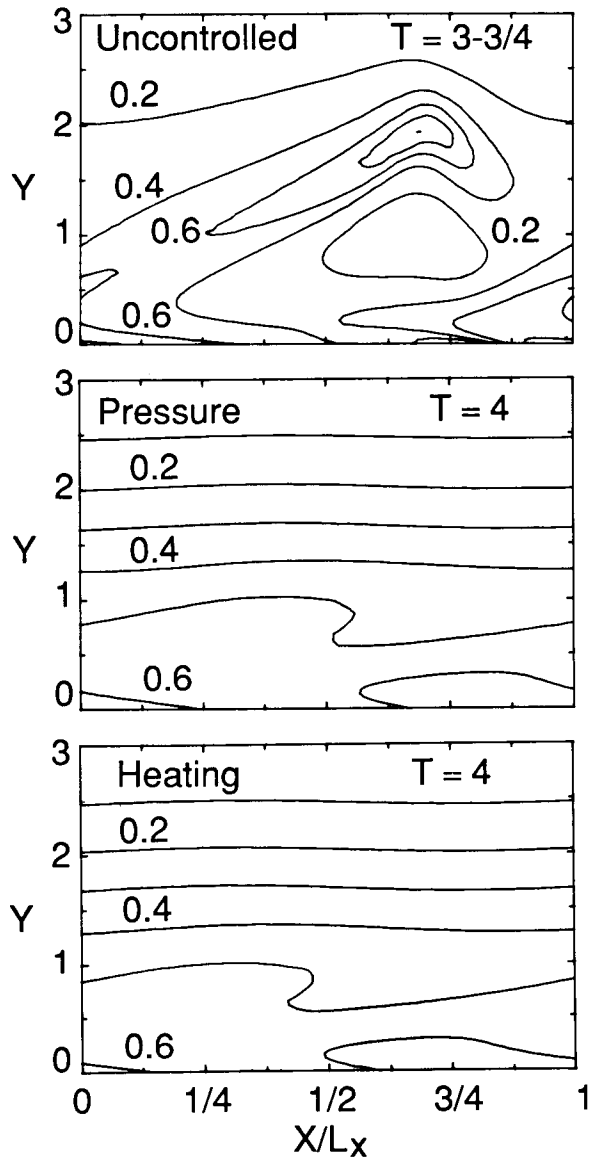

Fig. 11. Vertical shear $\partial u/\partial y$ in the peak plane for boundary layer simulations with initial two-dimensional TS amplitudes of 1.8%. Lengths are scaled by displacement thickness.

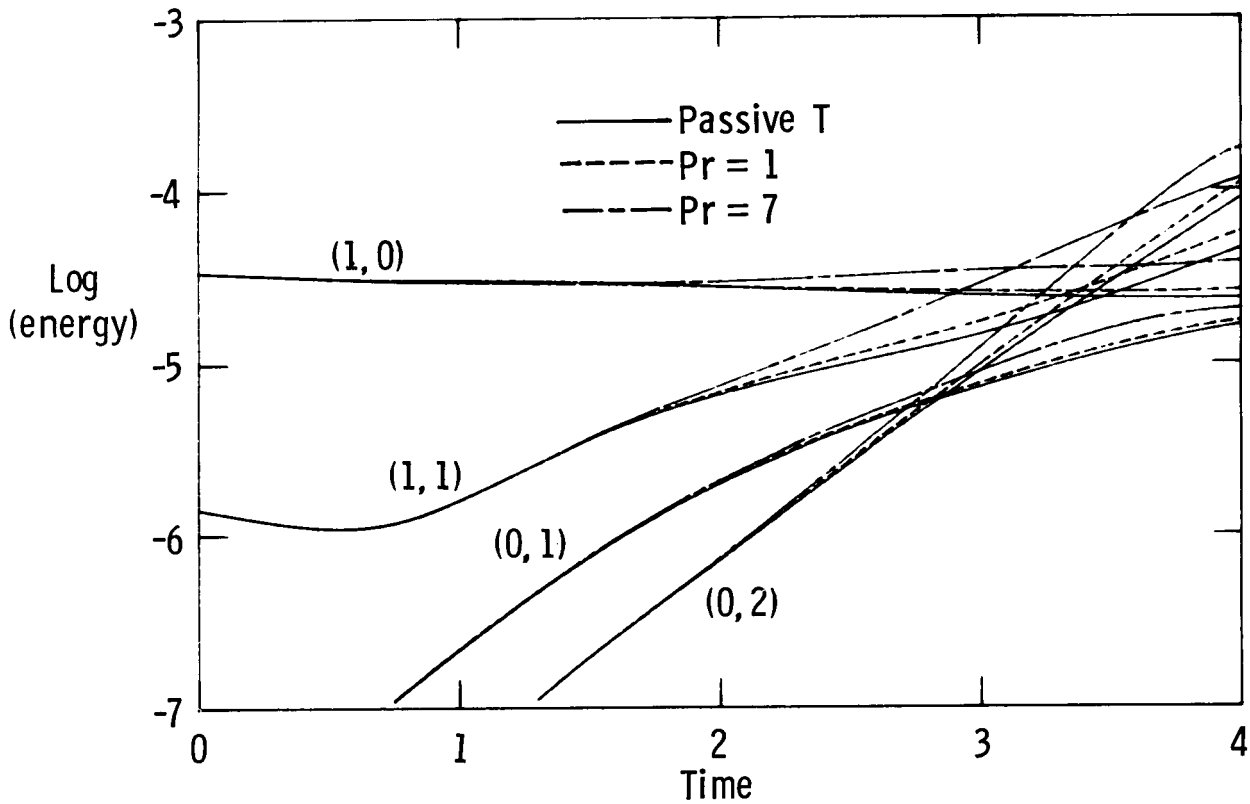

Fig. 12. Harmonic history for heated boundary layer simulations with initial two-dimensional TS amplitudes of 2.7%.

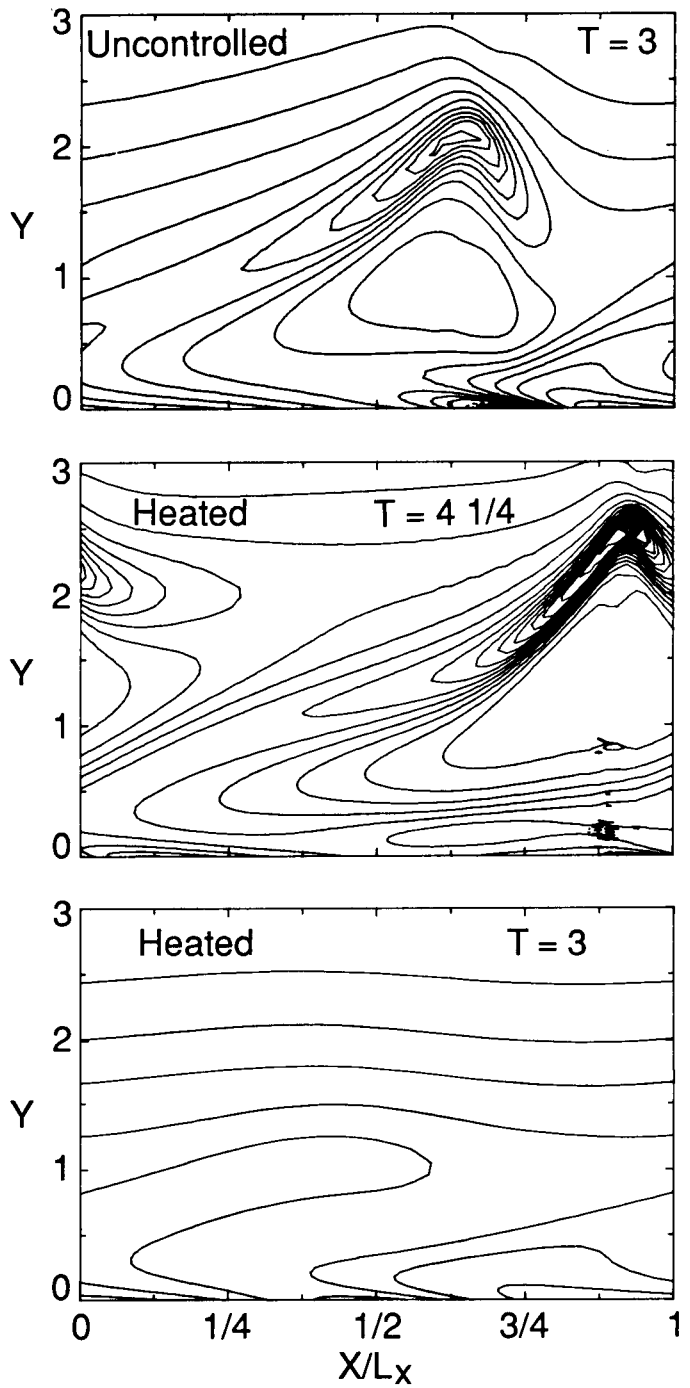

Fig. 13. Vertical shear in the peak plane for Re = 1100 boundary layers with ε_2 = .027.

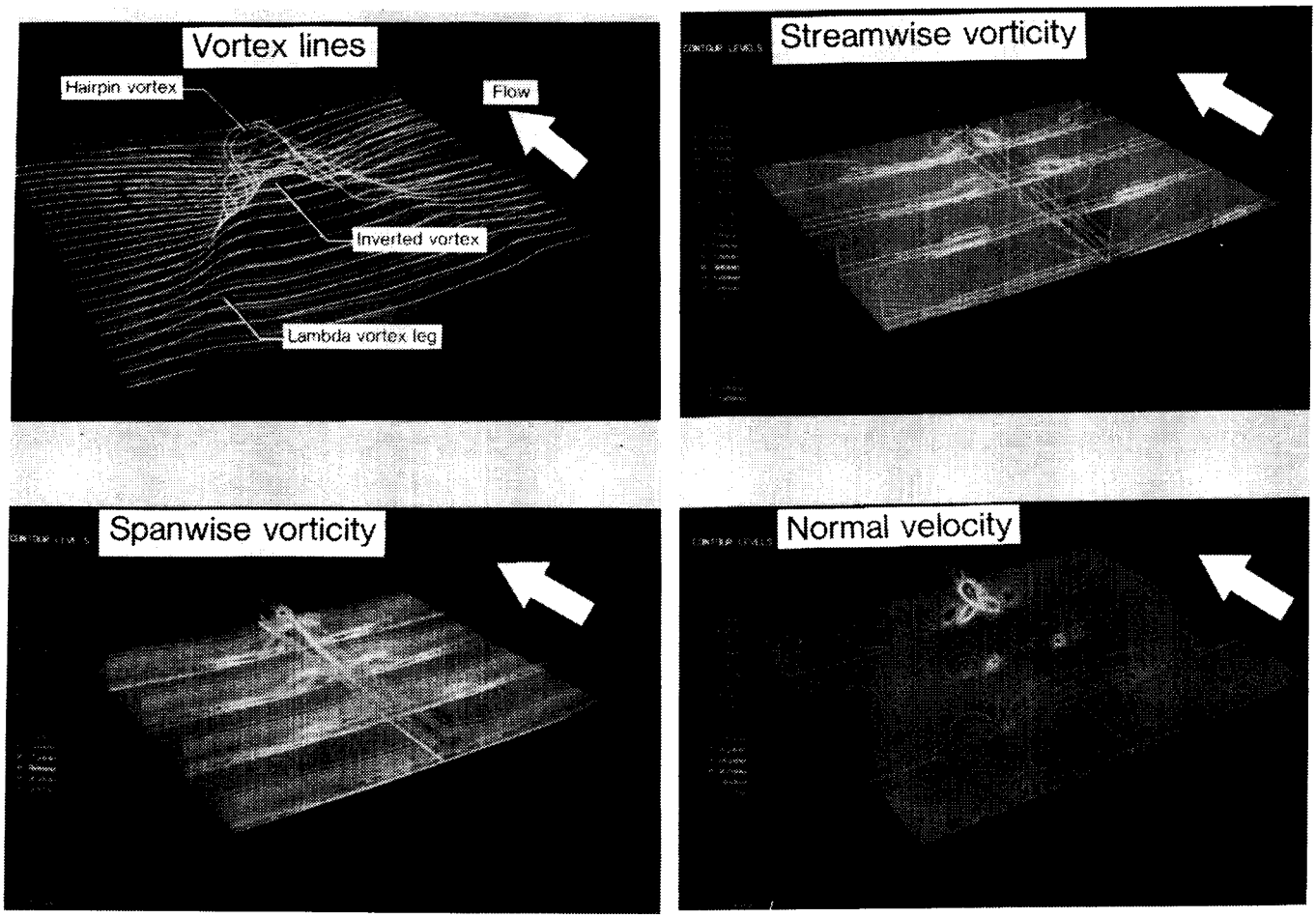

Fig. 14. Flow field after $3\frac{7}{8}$ periods for the Re = 1100 boundary layer transition.

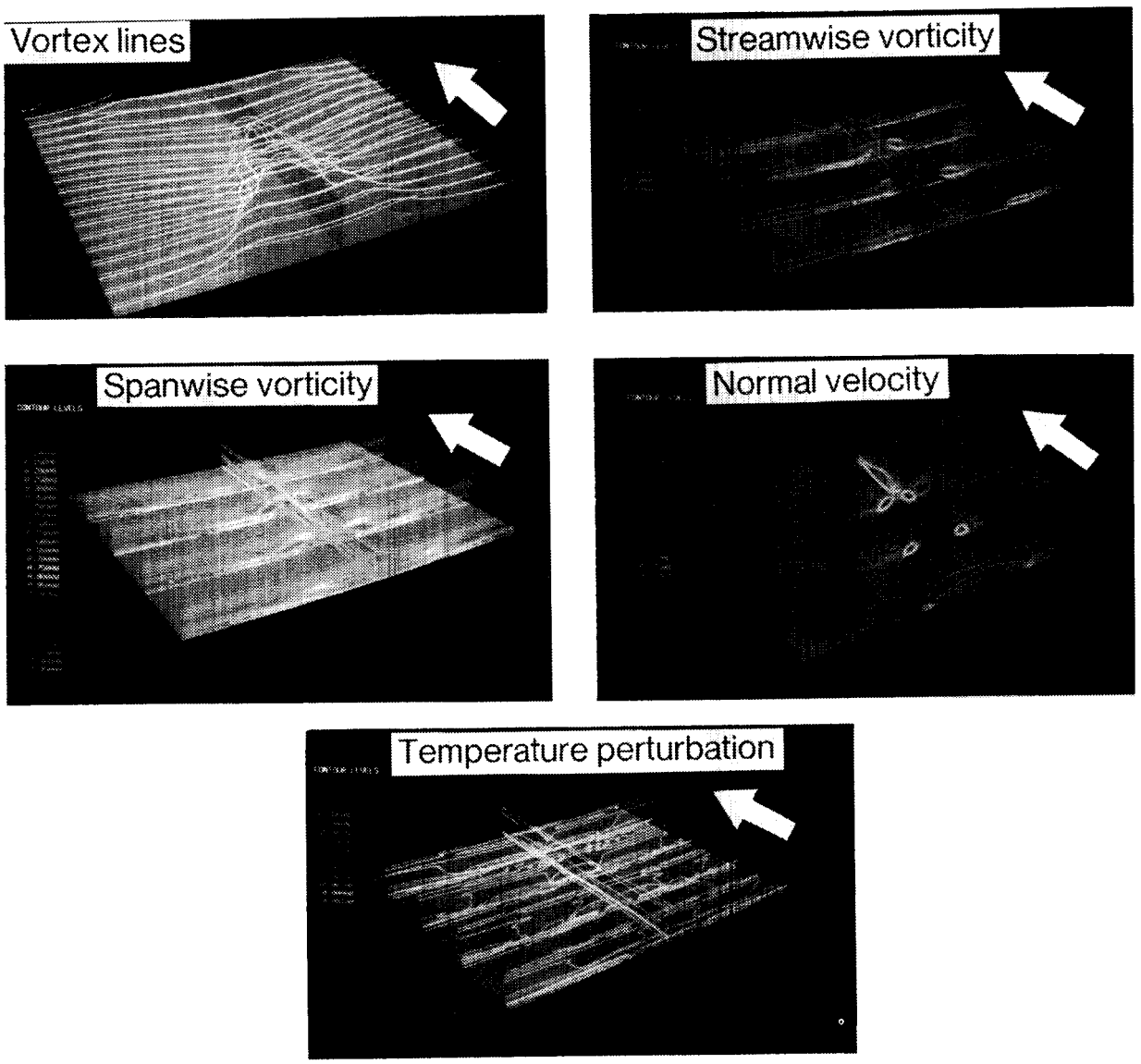

Fig. 15. Flow field after $4\frac{1}{4}$ periods for the Re = 1100 heated boundary layer transition.

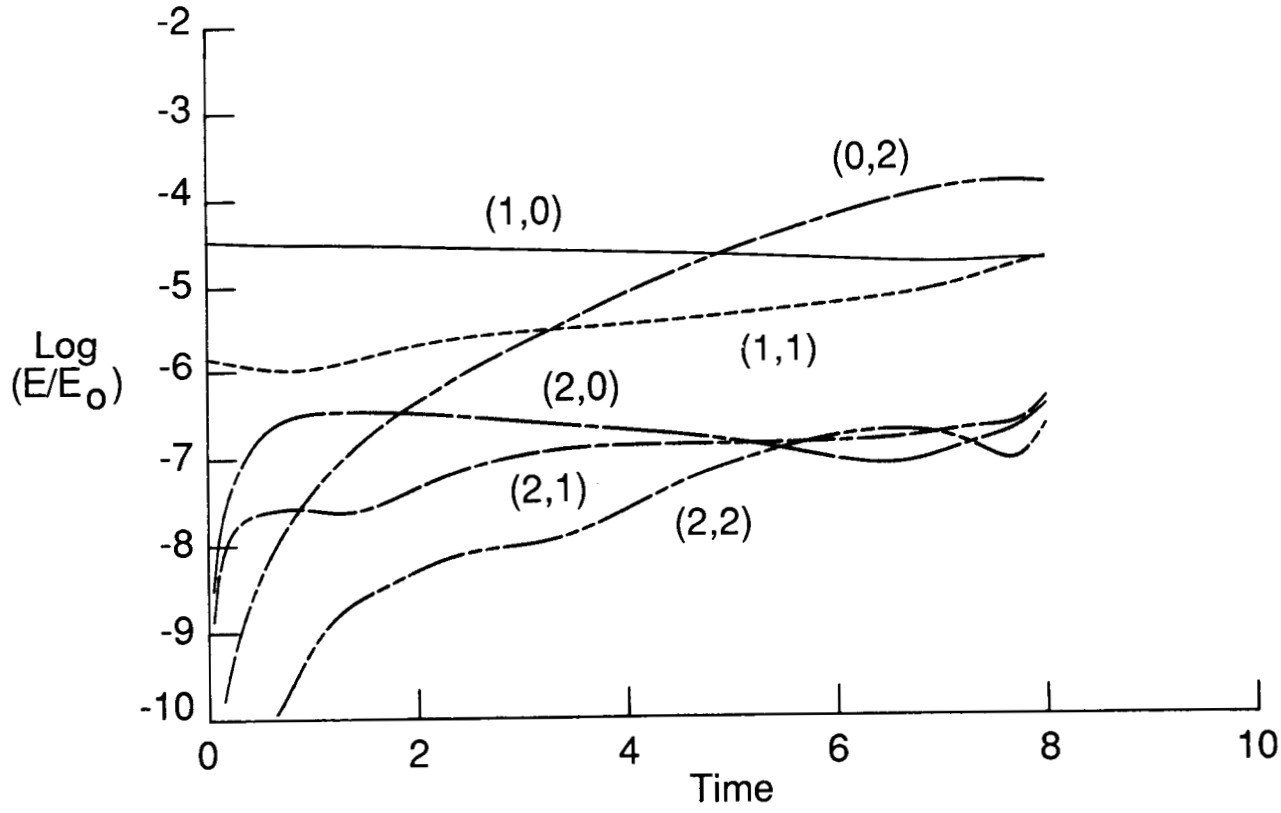

Fig. 16. Harmonic history for a Re = 1100 heated boundary layer simulation with an initial two-dimensional TS amplitude of 2.7%, but with the spanwise mode suppressed.

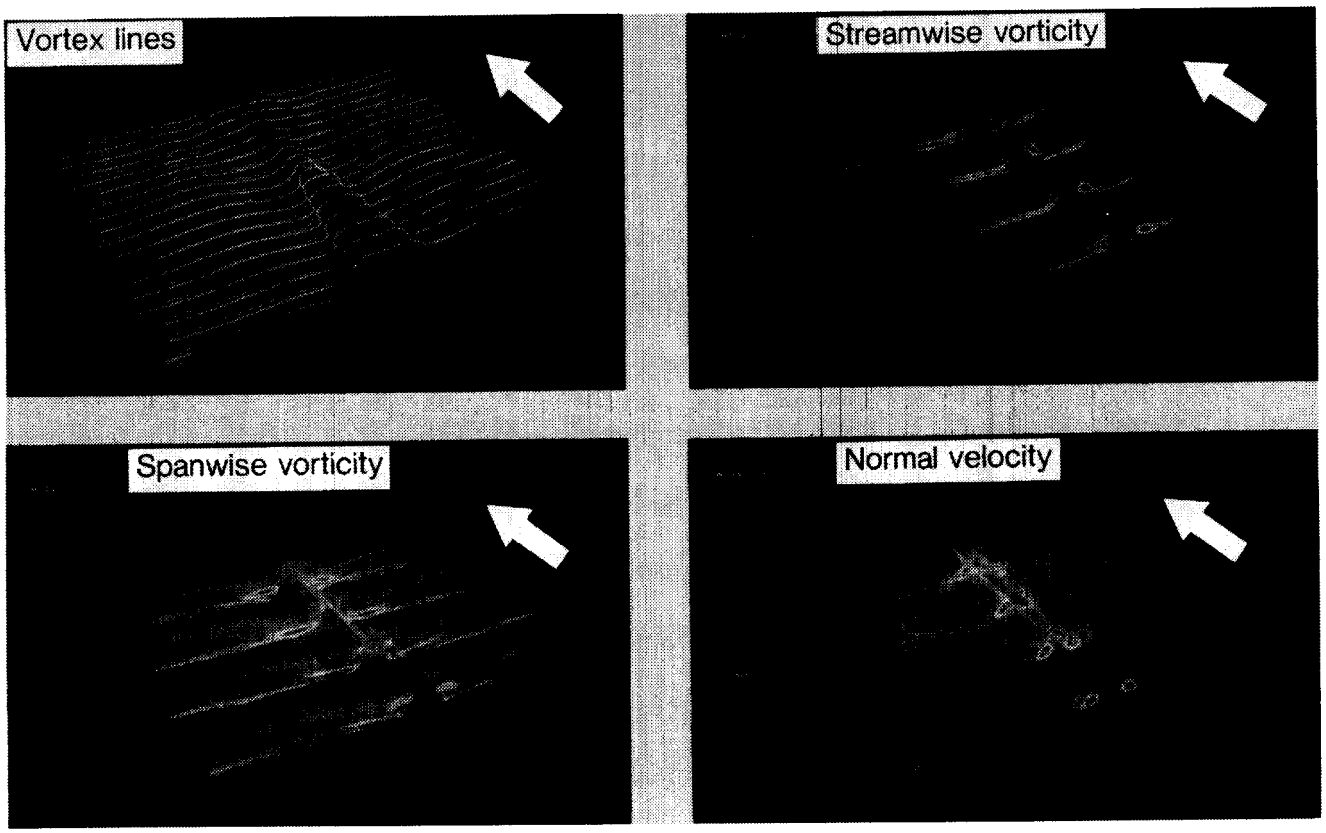

Fig. 17. Flow field after 8 periods for the Re = 1100 boundary layer transition with the spanwise mode suppressed.

NASA
National Aeronautics and Space Administration

Report Documentation Page

1. Report No.	2. Government Accession No.	3. Recipient's Catalog No.
NASA CR-181649 ICASE Report No. 88-20		

4. Title and Subtitle	5. Report Date
NUMERICAL EXPERIMENTS ON THE STABILITY OF CONTROLLED BOUNDARY LAYERS	March 1988
	6. Performing Organization Code

7. Author(s)	8. Performing Organization Report No.
Thomas A. Zang and M. Y. Hussaini	88-20
	10. Work Unit No.
	505-90-21-01

9. Performing Organization Name and Address	11. Contract or Grant No.
Institute for Computer Applications in Science and Engineering Mail Stop 132C, NASA Langley Research Center Hampton, VA 23665-5225	NAS1-18107
	13. Type of Report and Period Covered
12. Sponsoring Agency Name and Address	Contractor Report
National Aeronautics and Space Administration Langley Research Center Hampton, VA 23665-5225	14. Sponsoring Agency Code

15. Supplementary Notes

Langley Technical Monitor:
Richard W. Barnwell

Submitted to J. Fluid Mech.

Final Report

16. Abstract

Nonlinear simulations are presented for instability and transition in parallel water boundary layers subjected to pressure gradient, suction, or heating control. In the nonlinear regime, finite amplitude two-dimensional Tollmien-Schlichting waves grow faster than is predicted by linear theory. Moreover, this discrepancy is greatest in the case of heating control. Likewise, heating control is found to be the least effective in delaying secondary instabilities of both the fundamental and subharmonic type. Flow-field details (including temperature profiles) are presented for both the uncontrolled boundary layer and the heated boundary layer.

17. Key Words (Suggested by Author(s))	18. Distribution Statement
Navier-Stokes equations, stability of water boundary layers, laminar flow control	34 - Fluid Mechanics and Heat Transfer 64 - Numerical Analysis Unclassified - unlimited

19. Security Classif. (of this report)	20. Security Classif. (of this page)	21. No. of pages	22. Price
Unclassified	Unclassified	51	A04

NASA FORM 1626 OCT 86